CHALMERS
UNIVERSITY OF TECHNOLOGY

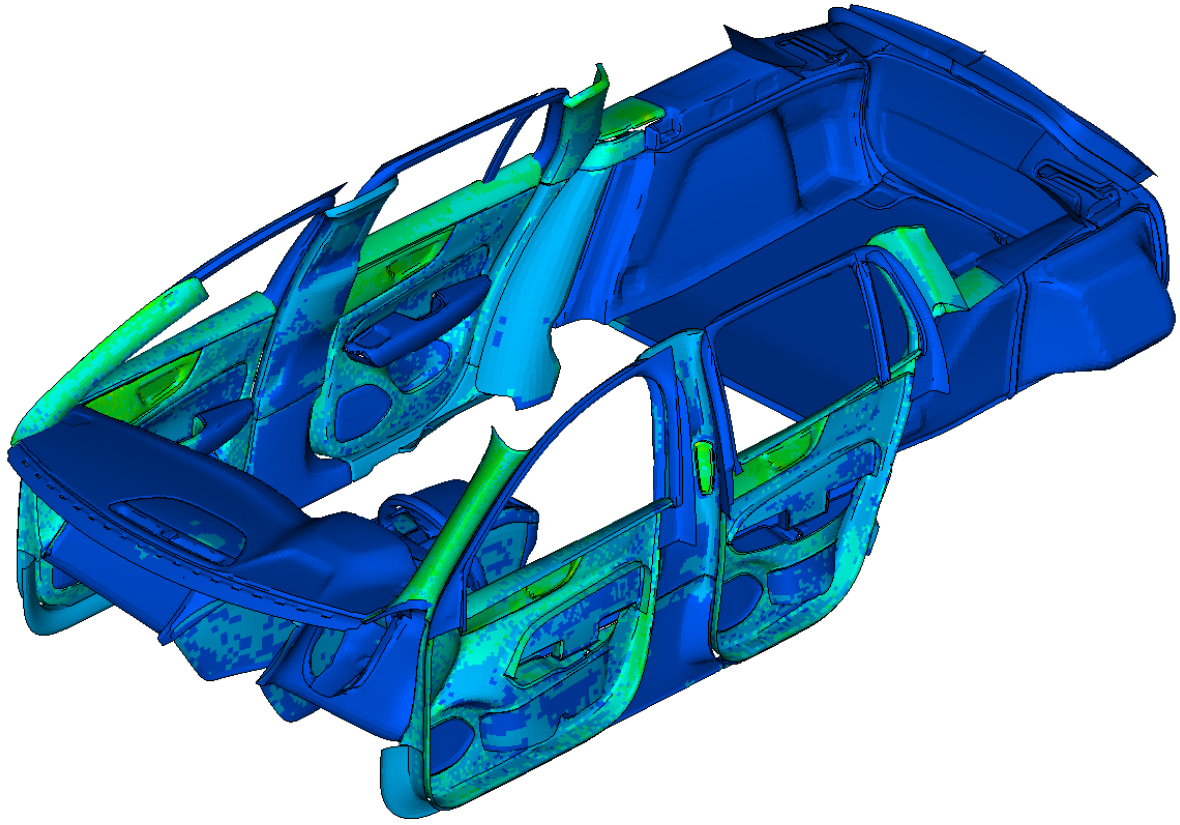

Holistic Sun Simulation of Polymer Materials in Automotive Applications

Master's thesis in Applied Mechanics

KRISTIAN IVANCIC

DEPARTMENT OF INDUSTRIAL AND MATERIALS SCIENCE

CHALMERS UNIVERSITY OF TECHNOLOGY
Gothenburg, Sweden 2021
www.chalmers.se

Master's thesis 2021

Holistic Sun Simulation of Polymer Materials in Automotive Applications

KRISTIAN IVANCIC

CHALMERS
UNIVERSITY OF TECHNOLOGY

Department of Industrial and Materials Science
Division of Material and Computational Mechanics
Chalmers University of Technology
Gothenburg, Sweden 2021

Holistic Sun Simulation of Polymer Materials in Automotive Applications
KRISTIAN IVANCIC

Supervisor: Renaud Gutkin, Volvo Cars Corporation
Examiner: Prof. Leif Asp, Department of Industrial and Materials Science

Master's Thesis 2021
Department of Industrial and Materials Science
Division of Material and Computational Mechanics
Chalmers University of Technology
SE-412 96 Gothenburg
Telephone +46 31 772 1000

Cover: Visualization of von Mises stress from sun simulation of a full car model.

Typeset in LaTeX
Printed by Chalmers Reproservice
Gothenburg, Sweden 2021

Holistic Sun Simulation of Polymer Materials in Automotive Applications
KRISTIAN IVANCIC
Department of Industrial and Materials Science
Division of Material and Computational Mechanics
Chalmers University of Technology

Abstract

Deformation of components due to thermal loads caused by the sun light is an important aspect to consider in automotive interior trim design. The sun light may cause the cabin to heat up extensively, which may affect both the structural rigidity and cosmetics of the trim components. Currently, physical tests are carried out in order to measure the response from such thermal loads. However, studies are often both time and cost expensive. Previous work has shown that the response can be obtained through sun simulation. For such a simulation, weather data is used to predict the thermal loads, which are then applied on a full car model. Moreover, the simulation methodology enables the effect of customer vehicle usage to be taken into consideration.

The majority of vehicle interior trim components are made of polymer materials, as they offer cost efficient and lightweight solutions. For components with higher structural requirements, fibre reinforced polymers are often implemented. In order to be successful in the application of polymer materials, the thermal as well as mechanical behaviour of the polymer has to be taken into consideration. Furthermore, as most components are manufactured through injection moulding, process induced stresses and fibre orientations may also have an effect on the result. In order to increase the fidelity of the sun simulation model these factors have to be taken into consideration. Thus, this thesis presents the development of a workflow that allows process induced parameters to be used as an input when performing sun simulation on complete vehicle models.

A workflow has successfully been developed that allows for process induced parameters to be taken into account for structural analysis. Results show that process induced stresses and fibre orientations have an impact on the results obtained from sun simulations on complete car models.

Keywords: Injection moulding, Sun simulation, Residual stress, Fibre orientation, Warpage, Polymer, Automotive.

Acknowledgements

This thesis was made possible by Volvo Cars through guidance from my supervisors Renaud Gutkin and Björn Ratama, who have provided support throughout the project. They have both been a valuable source of knowledge and great forum for discussion. I would also like to thank my examiner Leif Asp for his valuable input and for introducing me to the project. Furthermore, thank you Heléne Carlsson and other employees from the CAE department at Volvo Cars, for answering my questions and providing help when needed.

In addition I would like to express my gratitude for the support from Moldflow, Moldex3D and Digimat, who have not only provided licenses for the process simulation software used in this project, but who have continuously been available for discussing options and ways forward. A big thank you to George Mokios who offered great support in the application of the pre-and post processing software provided by Beta Solutions and who enabled the development of new mapping functions in the Ansa pre-processing software.

Finally, I would like to thank my family for always supporting me in life and throughout my education.

Kristian Ivancic, Gothenburg, June 2021

Contents

List of Figures

1
Introduction

Polymer materials possess properties that make them useful in a variety of applications, ranging from products used in our daily life such as plastic bottles and bags to high performance applications such as orthopedics, dental and aerospace. The ductile and plastic characteristics of polymers make it possible to use low cost manufacturing methods, such as injection moulding, to form them into complicated shapes. Furthermore, polymers offer light weight solutions that are resistant to corrosion. For components with higher structural requirements, fibre reinforced polymers may be used [1].

During the last decade, the use of high performance plastics in automotive applications has increased rapidly, making up approximately 10 % of the total weight of the car [2], [3]. However, to be successful in the application of polymer materials, the behaviour during mechanical as well as thermal loading has to be understood. This thesis thus aims to improve the fidelity of full car structural analysis by taking process induced material properties into account.

1.1 Background

The work conducted for this thesis is the second part of a two-thesis project. The first part of the project aimed towards developing a way of simulating the effect of the sun load on vehicle interior trim components during one year of customer usage [4]. The software TAITherm was used to successfully compute thermal loads from weather data. The transient thermal load was then applied on a complete car model for which a structural analysis was performed.

The components used for the vehicle trim parts considered in this thesis are made of ABS, PP and PC type polymer materials, as shown in Figure 1.1. Furthermore, the components shown in the same figure are mainly manufactured by injection moulding. It is known that injection moulding process has a substantial effect on the mechanical and thermal properties of the final product [5]. The ever changing temperature of the mould and polymer during the manufacturing process gives rise to residual stresses.

The stresses are introduced as the polymer melt cools down and solidifies, which may cause defects such as distortion and cracking [6]. It may also cause cosmetic imperfections. Moreover, for fibre-reinforced polymers the flow of liquid polymer through the mould cavity determines the fibre orientations in the finished product, which causes anisotropic material behaviour [7].

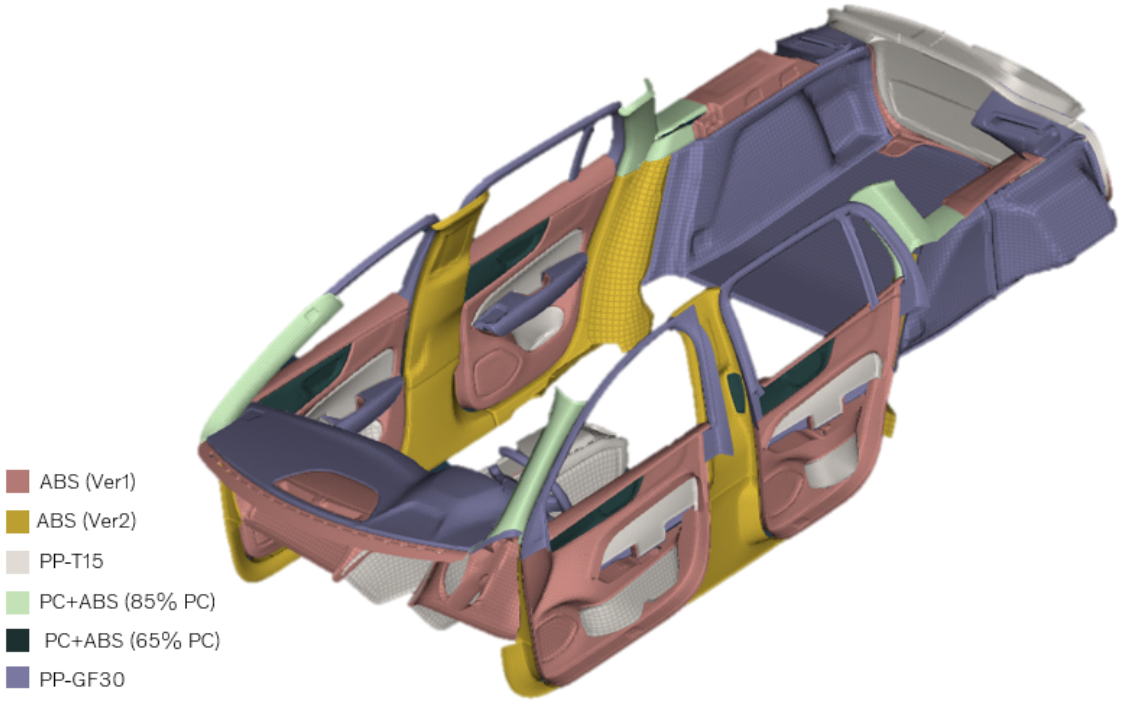

Figure 1.1: Visualization of the material-types used for the considered components in the full car model, image from [5].

The progression of Computer Aided Engineering (CAE) has made it possible to simulate the manufacturing process in order to improve the design process [6]. Earlier work has shown that residual stresses and fibre orientation can be computed with acceptable validity for certain components [8]. Furthermore, it has been shown that the process induced parameters may be used as initial conditions in structural analysis, having an effect on nodal warpage and final residual stresses in finished components [9]. It has also been shown that the residual stresses have an effect on the eigenfrequencies of such components [10]. Nevertheless, earlier studies have mainly focused on the response of one single component with minor regard to the usage and integration of the part with respect to its surrounding environment during its lifecycle. This thesis aim to couple the process of obtaining process induced parameters with the computation of structural response in a full car sun simulation model, with consideration to the customer usage of the vehicle.

1.2 Purpose

The purpose of this project is to expand the current knowledge regarding the effect of process induced properties on polymer material components by carrying out the full chain of simulations for a sun analysis. This includes simulations to be made of the injection moulding manufacturing process for all trim components considered in a complete car model. Additionally, the relaxation of all components is to be accounted for before stresses are used as initial conditions in the structural analysis. As the process of obtaining the sun load and transferring it to the structural solver is already established, the aim of the thesis is to include- and evaluate the effect of process induced properties on a sun simulation.

1.3 Objectives

The objective of this study is to carry out the full workflow for a sun simulation performed on a complete car model, including simulations for obtaining process induced material parameters. The objective can be divided into the sub goals listed below:

- Develop a new framework enabling a holistic analysis of polymers, including process induced properties, in complete car simulation.
- Define the best approach to obtain process induced properties for a large number of components.
- Evaluate the effect of introducing process induced parameters in the complete car model when performing a sun simulation.

1.4 Boundaries

This thesis work emphasizes the study and development of a method that enables the full chain of simulations to be carried out for a sun simulation of a full vehicle model. The results obtained from the structural analysis made with consideration to process induced properties is compared only with results obtained from carrying out a similar simulation without process induced properties. This means that no physical tests will be carried out.

It should further be noted that Moldflow, Moldex3D and Digimat will be the software used and evaluated for simulating the injection moulding process. No other software will be examined. Possibilities of obtaining other necessary software requirements with the tools available, such as mapping, are considered in the scope of the thesis. The structural analysis will be carried out using the Abaqus solver. Thus, the solution is limited to the possibilities of the chosen solver. Moreover, the pre- and post-processing will be done using the commercial software Ansa and Meta, respectively.

1.5 Method

The purpose of this thesis is to carry out the full chain of simulations, shown in Figure 1.2, for a sun simulation made on a complete car model, with consideration to process induced stresses and fibre orientations. The goal is thus to find a workflow that can be integrated in the use of the current models used for structural analysis. As seen in Figure 1.2, the process simulation and mapping is carried out per component. Accordingly, input data is defined for each component respectively. The structural analysis and evaluation of results is done for the full car model. The workflow is developed by using one component throughout the chain of simulations, after which it is carried out with all interior trim components considered.

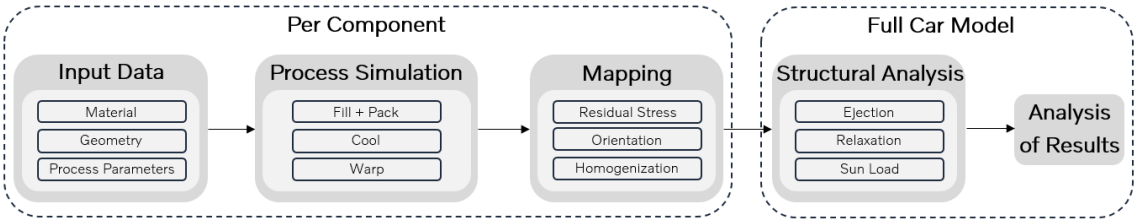

Figure 1.2: Full chain of simulations.

First, process parameters and material data is defined by consultation with the CAE department at Volvo Cars as well as with the process simulation software providers. Thereafter, the injection moulding is simulated for all software considered for this thesis. This is done for both a three-dimensional model and a midplane approximation. The results are then analyzed, after which an approach for further analysis is chosen. After obtaining the process induced parameters the data is transferred to the model used for the structural analysis. By collaborating with software providers a mapping function is developed and integrated into the workflow. When the mapping function has been established, the results are transferred to the full vehicle model.

A structural analysis is then performed on the full vehicle model with process induced properties for the test component. After successfully establishing the workflow, the procedure is repeated for all trim components seen in Figure 1.1. The sun simulation is then performed for a complete vehicle model with process induced parameters for all components manufactured by injection moulding.

2

Manufacturing Process and Material Behaviour

2.1 Polymer Injection Moulding

The most commonly used manufacturing process for articles of polymer material is injection moulding. During the manufacturing process polymer granules are melted and fed into a mould cavity under high pressure. By cooling down the mould the polymer solidifies and can be ejected in the shape of the desired article. The advantage of using injection moulding is the capacity of reproducing a large number of identical articles regardless of the complexity of the geometry [5].

2.1.1 Manufacturing Process

The machine used for injection moulding consists of an injection unit and a clamping unit. As seen in the upper illustration of Figure 2.1, the injection unit consists of a hopper, heated barrel and rotating screw, whereas the clamping unit consists of a mould, which is usually made of two halves.

The first stage of the injection moulding process, seen in the top of Figure 2.1, is the plastification phase. In operation, polymer granules are fed into the machine through the hopper and pushed forward through the screw channels [7]. As the screw rotates the mechanical energy forces the granules against the wall. The granules then melt both due to the friction heat generated by the rotating screw and conduction from the heating units placed along the barrel [5]. The liquid polymer accumulates in the area in front of the screw and is continuously heated in order to maintain the desired temperature.

After the desired volume of molten polymer has been obtained, the injection phase begins. This phase consists of filling, packing, cooling and ejection. In Figure 2.1, cooling is considered within the ejection phase.

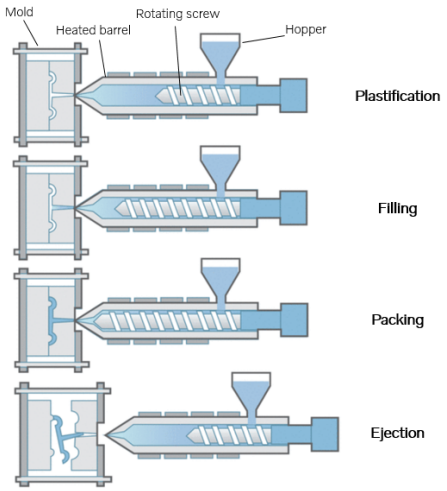

Figure 2.1: The injection moulding process, image from [7].

In the *filling* phase the mould is kept closed by the clamp unit while the screw moves forward and forces the liquid polymer into the mould cavity. The heated barrel, as well as the shear forces, causes the temperature to rise, as can be seen in Figure 2.2. Furthermore, the pressure also increases during the *filling* phase. When the mould is filled, the *packing* phase begins. The screw is held in its foremost position in order to maintain the desired pressure as the polymer cools down, which is shown by the pressure curve presented in Figure 2.2. In order to compensate for the volumetric shrinkage the screw may move forward with a small displacement, which causes more liquid material to enter the mould cavity. During the end of the *packing* phase the mould gates completely freeze. However, as seen in Figure 2.2, the part continues to cool down and solidify. This stage of the injection moulding process is called the *cooling* phase. The last stage of the manufacturing process is the *ejection* phase. When adequate time for cooling has past and the part has solidified to a point where it is stiff enough to be ejected, the mould cavity opens and the part is removed. The mould is then cooled and the process is repeated for the next article. [5] [7]

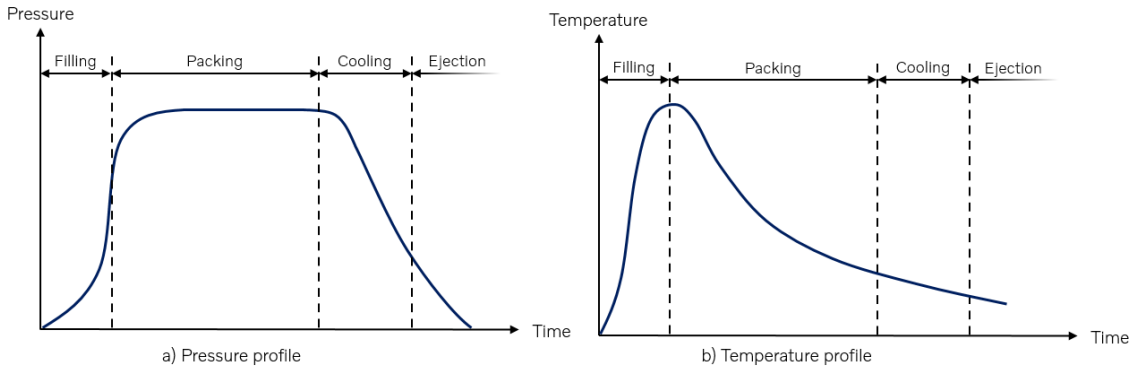

Figure 2.2: General pressure and temperature profile during injection moulding [11].

During the injection moulding process the material is heated, reshaped and cooled down, which affect the material properties. Furthermore, it induces stresses and deformations. Moreover, some of the components manufactured by injection moulding at Volvo Cars are made of composite materials. This means that the material is made up of two or more components. The properties are then dominated by the microstructure of the fabricated part rather than of the constituent materials [5]. In order to obtain the desired dimensional tolerances as well as mechanical-, thermal- and other properties in the final product, the rheology and properties of the materials used need to be understood.

2.1.2 Rheology and Material Properties of Polymers

The manufacturing process has a critical impact on the shape, dimensional tolerances and surface finish of the finished component. In order to understand the effect of the injection moulding process, the relations between deformation, temperature and applied stress within the material has to be understood [5]. Furthermore, the influence of the thermal and mechanical loads, as well as the impact of the process induced properties, plays a significant part in the properties of the final product. In order to understand how the different factors influence the material properties of the final article and thus the results obtained from a complete car sun simulation, the rheology of polymers has to be studied.

2.1.2.1 Classification of Polymers

The characteristics of polymers and results obtained from manufacturing by injection moulding largely depend on the structure of molecular chains. For the materials used in the scope of this thesis, the polymer chains are mainly linear or with chemical groups forming branches along the primary chain, as seen in Figure 2.3.

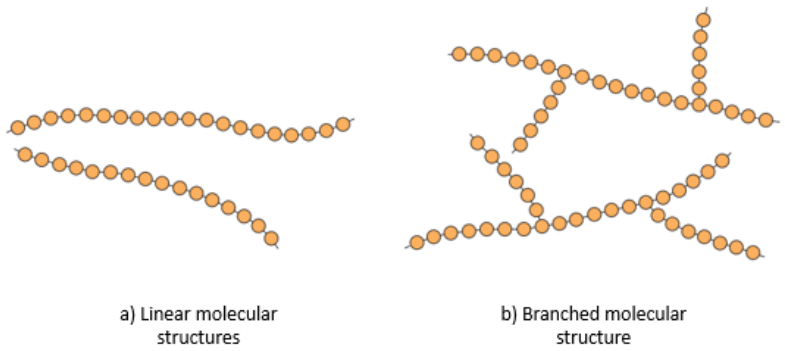

Figure 2.3: Schematic representation of linear and branched molecular structures, image from [12].

The polymer macromolecules are made up of a large number of molecular chains [5]. Each molecular chain consists of several repeat units, which in turn originates from monomers [12]. The monomers are joined together by covalent bonds and polymerization of one kind of monomer results in a homopolymer. However, if a polymer is made up of different types of monomers, it is called a copolymer.

The formation of the molecular structures affect the properties of the polymer material. The different molecular structures shown in Figure 2.3 are presented below. However, it should be noted that polymers most often do not consist of one single structural type. Rather they are made up of several types of polymer structures where some may be dominant [12].

- **Linear Polymers:**
  Linear polymers are the simplest form of polymers. In such a polymer, the carbon-carbon bonds are connected in one line [13]. Figure 2.3 a) shows a schematic representation of such a polymer, where each circle represents a repeat unit.

- **Branched Polymers:**
  Some polymers may have side-branch chains connected to the main ones. The branches may result from side reactions that occur during the synthesizaiton of the polymer. Such synthesized polymers are called branched polymers and can be seen in Figure 2.3 b) [12]. When heated, branched as well as linear polymers soften. This is a result of the higher temperature causing increased vibrations that overcome the attractive forces between the molecules [13].

The molecular structure affects the response of a polymer to mechanical forces and temperature. Based on their behaviour, polymers can be classified as either *Thermoplastics* or *Thermosets*. The thermoplastic polymers, as opposed to the latter, soften when heated and ultimately become liquid. Furthermore, they solidify when cooled. The process of liquefying and solidifying a thermoplastic polymer is fully reversible and repeatable. The polymers used for vehicle trim components, which are part of this study, are mainly thermoplastics. These may be both linear and branched in their molecular structure. Thus, no components mainly consisting of thermosetting polymers are part of this study.

Furthermore, thermoplastics can be divided into amorphous, semi-crystalline and liquid crystalline polymers based on the arrangement of molecular chains within the material. As presented in Figure 2.4, the molecular chains of amorphous polymers are randomly arranged. When cooled to the glass transition temperature T_g, the material changes from its rubber-like format to glass-like state [5]. Crystallizable polymers may under certain conditions align the molecular chains in an ordered way. For such polymers the cooling most often start from the melt phase which may result in only partial crystallization. Hence, the material may possess both amorphous and crystalline molecular structures and is thus called semi-crystalline [5]. When the molecular chains are in order in the melt state, as can be seen in

Figure 2.4 b), the polymer is liquid crystalline.

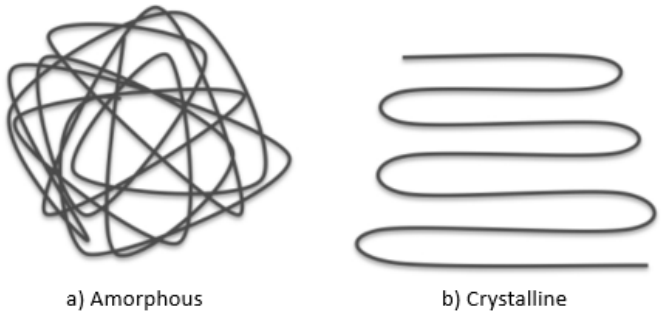

Figure 2.4: Amorphous and crystalline molecular chains, image from [12].

2.1.3 Rheological Characterization

The rheological properties of the polymer plays a significant role both in manufacturing and material characteristics. The behaviour of the polymer governs flowing resistance, required injection pressure, desired temperature and ultimately how the mould cavity is filled [7]. Furthermore, it affects the shrinkage, warp and deformation of the material which may cause residual stresses that disturb the results obtained from structural analysis.

2.1.3.1 Viscosity

The viscosity of a fluid is a measure of its resistance to flow or deformation, which affect manufacturing results. For a Newtonian fluid flowing in between two parallel walls, the viscosity η is defined according to Equation (2.1), where τ is the shear stress and $\dot{\gamma}$ is the shear rate [14]. The shear rate is obtained through Equation (2.2), where U is the constant wall velocity and h is the distance between two parallel plates. The shear stress is computed according to Equation (2.3), where F is the force applied and A is the cross sectional area of the material parallel to the force vector.

$$\eta = \frac{\tau_{12}}{\dot{\gamma}} \tag{2.1}$$

$$\dot{\gamma} = \frac{U}{h} \tag{2.2}$$

$$\tau_{12} = \frac{F}{A} \tag{2.3}$$

The flow of Newtonian fluids is characterised by the Navier-Stokes equation. For such fluids the shear stress is directly proportional to the shear rate [5]. The viscosity is thus a constant based on temperature, composition and pressure [7]. However, most thermoplastics are non-Newtonian fluids. Thus, their flow behaviour does not follow the Navier-Stokes equations. The flowing resistance of such a polymer is dependent on the orientation and structure of the molecular chains. As the orientation

of the molecular chains is affected by the flow, the viscosity changes with shear rate, as seen in Figure 2.5 [7].

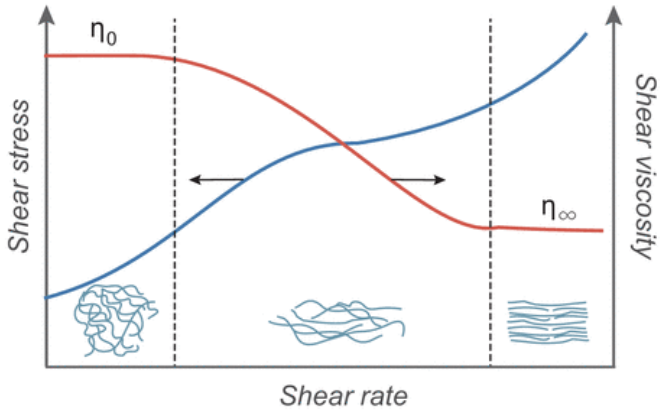

Figure 2.5: Shear viscosity and shear stress versus shear rate for non-Newtonian fluids, image from [7].

Such polymers can either behave as shear thinning fluids, meaning that the viscosity decreases with increased shear rate, or shear thickening fluids, meaning that the viscosity increases with an increase in shear rate.

The viscosity for non-Newtonian fluids is thus material-dependent. The materials used for the process simulation of vehicle trim parts is shown together with the full vehicle model in Figure 1.1. The viscosity model used for all materials considered in the work conducted for this thesis is the Cross-WLF viscosity model shown in Equation (2.4) [15]. Here, η is the melt viscosity, η_0 is the zero shear viscosity, $\dot{\gamma}$ is the shear rate, τ^* is the critical shear stress at the transition to shear thinning and n is the power law index in the high shear rate regime.

$$\eta = \frac{\eta_0}{1 + \left(\frac{\eta_0 \dot{\gamma}}{\tau *}^{1-n}\right)} \tag{2.4}$$

The zero shear viscosity η_0 is obtained from Equation (2.5), where T is the temperature in Kelvin, T^* is the glass transition temperature and D_1, A_1 and A_2 are determined by data fitted coefficients.

$$\eta_0 = D_1 e^{\left[-\frac{A_1(T-T^*)}{A_2+(T-T^*)}\right]} \tag{2.5}$$

2.1.3.2 Viscoelastic Behaviour of Fluid Polymers

Polymers often possess a combination of viscous and elastic material properties. The deformation of a pure elastic material subjected to a force is considered instantaneous and returns to its original shape when the force is removed. However, for a pure viscous fluid a deforming force will cause permanent rearrangement of the molecular structures. For such a case the deformation will be time dependent and irreversible. [5]

Since the behaviour of polymers is often in-between that of an elastic solid and viscous liquid, the material is called a viscoelastic fluid [5]. In such a case an applied stress load first result in an instantaneous elastic strain where after a time-dependent strain occur [12]. Viscoelastic liquid polymers generally show shear rate dependent properties. As the shear rate increases the molecular chains untangle and become more uniformly oriented, see Figure 2.5. Since the entanglement of the molecular chains itself has a major impact on the flowing resistance of the material, the viscosity decreases as the shear rate increases. Vastly increased shear stress may cause the molecular chains to deform and eventually break, which leads to a decrease in viscosity and degradation of the polymeric material. [7]

2.1.3.3 Thermal Properties of Polymers

During the plastification phase of the injection moulding process, the polymer granules are heated to their melt state. The temperature of the polymer injected into the mould cavity during the filling phase should be higher than the melting temperature T_m. However, after the ejection phase the polymer has to be cooled down to a temperature below the glass transition temperature T_g of the material for the solidification of the component to be ensured. This process implicates that the polymer material is heated above its melt stage and then cooled down below its glass transition state during a short time interval. Thus, the thermal conductivity k and specific heat capacity C_p of the material has a significant impact on the results. [7]

As the density and volume of the material changes with pressure and temperature, the specific heat capacity may be defined as presented in Equation (2.6), where Q is the thermal energy and fixed pressure is assumed. The relationship between temperature, pressure and volume follows the PVT relation. [7]

$$C_P = \left(\frac{dQ}{dT} \right)_P \tag{2.6}$$

2.1.3.4 The Pressure - Volume - Temperature Relation

The equation of state for thermoplastic polymers follows the 2-domain Tait PVT model shown in Equation (2.7), where $v(T, p)$ is the specific volume as a function of temperature and pressure. Here, v_0 is the specific volume at zero gauge pressure, T is the temperature in Kelvin, p is the pressure in Pa, C is a constant specified to 0.0894 and B is a parameter accounting for the pressure sensitivity of the material [14], [15]. The 2-domain Tait PVT model is used for all material models in this project [15]. PVT diagrams for all materials used for the full car simulation are presented in Appendix A.1-A.6.

$$v(T,p) = v_0(T)\left[1 - C\,ln\left(1 + \frac{p}{B(T)}\right)\right] + v_t(T,p) \tag{2.7}$$

2.1.4 Flow Evolution

As the liquid polymer travels through the mould cavity the advancing flow front shows the fountain flow effect [5]. This can be seen in Figure 2.6, which presents a cross section of a flow channel close to the flow front. Here, it is noted that the fluid particles decelerate as they move towards the flow front, after which they roll over towards the walls. As can be seen in the same figure, the flow may be divided into a core- and skin subregion [5]. In the core subregion the relative velocity field is positive while in the skin subregion it is negative. Between the two layers the velocity vectors are close to zero in all directions, giving rise to a neutral line. It has been shown that the fountain flow effect has a major impact on the melt-front temperature as well as orientation distribution for fibre-filled components [16].

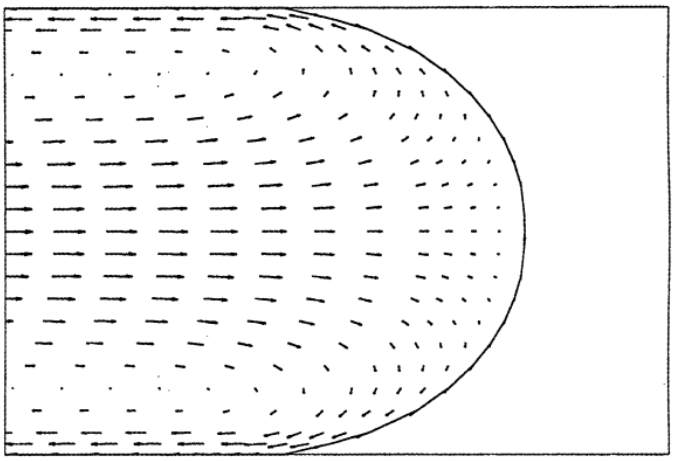

Figure 2.6: The fountain flow velocity vector field in a moving frame of reference, image from [5].

2.1.5 Stress Development

In order to fully understand and predict the dimensional and shape inaccuracies of injection moulded articles the knowledge of residual stress is essential. The residual stresses are those caused by the injection moulding process, remaining in the material after ejection. As is the case of external load, the residual stresses cause the component to deform [5], [17]. The residual stresses are induced either by the pressure field, i.e. the flow of liquid polymer, or as a result of the ever changing temperature during the injection moulding process [5].

Due to the rheology of liquid polymer and its viscoelastic properties, stresses in the normal direction to the flow occur during the filling and packing phases of the injection moulding process [17]. Stresses caused by the flow are often called flow-induced

stresses. Although the flow-induced stresses are small in relation to thermal-induced stresses, they have a significant impact on the mechanical behaviour of the finished product, since the flow heavily affect the molecular orientations [5].

When the polymer is in its molten state, the molecular chains become unstressed and may reach the amorphous phase [5]. However, as the liquid polymer travels through the mould cavity the molecular chains are sheared and elongated. In the case of the deformations of molecular chains not being fully relaxed as the part solidifies, they tend to lock in their altered orientation, causing inherent stresses [5], [9].

The thermal induced stresses result from several reasons, the rapid increase in rigidity being the main cause [17]. As cavity walls transfer energy away from the molten polymer by conduction, frozen layers develop from the outer surface toward the core and contract as they solidify [5], [11]. This gives rise to a non uniform temperature distribution across the component, which causes each layer and material point to solidify at a different time and temperature, leading to differential shrinkage [5], [17].

In-cavity stresses build up as the part solidifies. However, there are several factors that prevent shrinkage from occurring when the component is in the mould. For example adhesion to the cavity walls restrains the outer skin from moving. Moreover, the newly formed solid surface is fixed by the stretching forces of the melt pressure [15]. Thus, it is assumed that no part-mould detachment and no in-mould shrinkage occurs. When the part is ejected, the built up stresses will release and cause shrinkage and deformation.

The strain and stress is computed incrementally, using the equilibrium shown in Equation (2.8). Here, C_{ijrs}, $e_{rs}^{ini(k)}$ and ${}^{t+\Delta t}S_{ij}^{(k-1)}$ are the stress-strain tensor, the incremental initial strain tensor and the second Piola-Kirschoff stress tensor after iteration $(k-1)$ at time $t+\Delta t$. Moreover, $\Delta e_{rs}^{(k)}$ and $\Delta\eta_{ij}^{(k)}$ are the linear and non-linear incremental strain tensors whereas $\delta\Delta e_{ij}^{(k)}$ and $\delta\Delta\eta_{ij}^{(k)}$ are the linear an non-linear incremental strain tensors corresponding to virtual displacement.

$$\int_v C_{ijrs}\Delta e_{rs}^{(k)}\delta\Delta e_{ij}^{(k-1)}dV + \int_v^{t+\Delta t} S_{ij}^{(k-1)}\delta\Delta\eta_{ij}^{(k)}dV = -\int_v^{t+\Delta t} S_{ij}^{(k-1)}\delta\Delta e_{ij}^{(k-1)}dV + \int_v C_{ijrs}\Delta e_{rs}^{ini(k)}\delta\Delta e_{ij}^{(k-1)}dV \quad (2.8)$$

The residual stress after shrinkage is computed as the sum of the initial stresses that stem from the frozen pressure at each node and initial stresses due to thermal shrinkage. Thus, Equation (2.9) is used to compute the residual stresses, where D_g is the stress-strain relationship tensor, ϵ_{g0} is the initial strain from zero pressure state and σ_{g0} is the initial stress occurring as a result of the pressure at freeze [15].

$$\sigma_g = -D_g\epsilon_{g0} + \sigma_{g0} \quad (2.9)$$

2.2 Thermal and Viscoelastic Polymer Behaviour

The response of the components depends not only on the manufacturing process, but also on the material properties. The viscoelastic, thermal and structural response causes deformations [5]. An applied load may for example cause an elastic or plastic strain response. Moreover, a fixed load under long time and constant temperature can give rise to creep, while a change in temperature may cause thermal expansion [5], [14]. Thus, the total strain of a component can be seen as the sum of these effects, according to Equation (2.10), where, ϵ^{tot}, ϵ^{el}, ϵ^{pl}, ϵ^{cr} and ϵ^{th} are the total-, elastic-, plastic-, creep- and thermal strain.

$$\epsilon^{tot} = \epsilon^{el} + \epsilon^{pl} + \epsilon^{cr} + \epsilon^{th} \tag{2.10}$$

2.2.1 Viscoelastic Behaviour of Solid Polymers

The viscoelastic phenomena of solid polymers can be described through stress relaxation and creep. The stress relaxation is a time dependent change in stress at a constant applied strain and temperature while creep is the increase in strain with time in response to a constant applied stress, also at constant temperature [5]. Furthermore, polymer materials have a tendency of partially returning to its former state after an applied load has been removed, which is characterized by its recovery [5].

As seen in the ideal creep curve presented in Figure 2.7, the creep behaviour can be divided into three regions [14]. When applying a load, there is initially an instantaneous elastic deformation. However, as time passes primary creep occurs first, characterized by a continuously decreasing strain rate, also known as strain hardening [14]. After the first region the stationary secondary region is entered, where the creep rate remains constant. This may be explained by a balance occurring between strain hardening and recovery. In the tertiary phase the creep rate increases and results in failure.

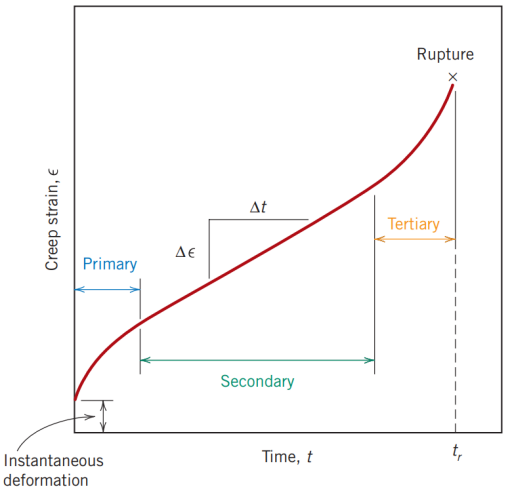

Figure 2.7: Ideal creep curve, image from [14].

For the purpose of this thesis the Time Power Law, seen in Equation (2.11), has been used to model the creep behaviour, where the equivalent creep rate $\dot{\bar{\epsilon}}^{cr}$ is defined according to Equation (2.12). Moreover, t is the total time during which the creep occurs, while A, n and m are series parameters which are fitted to material data. Finally, q is the von Mises effective stress, computed according to Equation (2.13), where $\boldsymbol{S}$ is the deviatoric stress defined according to Equation (2.14) and p is the pressure defined according to Equation (2.15).

$$\dot{\bar{\epsilon}}^{cr} = Aq^n t^m \tag{2.11}$$

$$\dot{\bar{\epsilon}}^{cr} = \sqrt{\left(\frac{2}{3}\dot{\boldsymbol{\epsilon}}^{\boldsymbol{cr}} : \dot{\boldsymbol{\epsilon}}^{\boldsymbol{cr}}\right)} \tag{2.12}$$

$$q = \sqrt{\left(\frac{3}{2}\boldsymbol{S} : \boldsymbol{S}\right)} \tag{2.13}$$

$$\boldsymbol{S} = \boldsymbol{\sigma} + p\boldsymbol{I} \tag{2.14}$$

$$p = -\frac{1}{3}trace(\boldsymbol{\sigma}) \tag{2.15}$$

2.2.2 Thermal Response of Polymer Materials

Under an increase in temperature, as is the case for a component being exposed to sun load, the material expands [18]. Furthermore, shrinkage and warpage occurring after the injection moulding process depend on the thermal properties of the polymer material [5]. The strain due to thermal loads ϵ^{th} can be defined according to Equation (2.16), where α is the coefficient of thermal expansion and ΔT is the increase in temperature.

$$\epsilon^{th} = \alpha \Delta T \tag{2.16}$$

2.3 Fibre-Reinforced Polymers

Car interiors use a wide range of material types in order to satisfy structural, thermal and aesthetic requirements. Many components produced by injection moulding are thus made from fibre-reinforced polymers in order to increase the strength and stiffness of the material [5]. For such components, the mechanical and thermal properties are highly dependent on the orientation and distribution of fibres, induced by the flow directions during processing [5]. Thus, in order to capture the effect of process induced properties in sun simulation, the fibre orientation and thermo-mechanical properties of fibre-reinforced polymers need to be understood.

2.3.1 Fibre Orientation Effect

The flow of fluid polymer through the mould cavity causes the fibre orientation to change, as the molecular structures are sheared and elongated [5]. Moreover, it has been shown that the fountain flow effect significantly affect the fibre orientation distribution, especially in the skin subregion close to the wall [16]. In order to describe the orientation of fibres, the probability density function $\Psi(\mathbf{p}, t)$ is used, where the direction is described by $\mathbf{p}$ and the time by t. The function thus describes the probability of finding a fibre oriented in a range between $\mathbf{p}$ and $\mathbf{p} + d\mathbf{p}$ at a given time t [5]. Furthermore, it should be noted that the integral of the probability density function over all values of $\mathbf{p}$ equals unity, meaning that Equation (2.17) must hold and that the range of the function is $[0, 1]$. Moreover, since the directions described by vectors $\mathbf{p}$ and $-\mathbf{p}$ effectively are the same, the distribution is considered even, meaning that Equation (2.18) holds [5].

$$\int \Psi(p, t)dp = 1 \tag{2.17}$$

$$\Psi(\boldsymbol{p}, t) = \Psi(-\boldsymbol{p}, t) \tag{2.18}$$

By using the probability density function, orientation tensors can be defined in term of the average of the dyadic products of the unit vector $\mathbf{p}$, as shown in Equation (2.19)-(2.20) [5]. The average of the dyadic product can then be defined according to Equation (2.21). Examples of the orientation tensor are shown for highly aligned-, partly aligned- and randomly distributed fibres in Figure 2.8.

$$a_{ij} \equiv < p_i p_j > = \int p_i p_j \Psi d\boldsymbol{p} \tag{2.19}$$

$$a_{ijkl} \equiv < p_i p_j p_k p_l > = \int p_i p_j p_k p_l \Psi d\boldsymbol{p} \tag{2.20}$$

$$< * > = \int * \Psi(\boldsymbol{p}, t) d\boldsymbol{p} \tag{2.21}$$

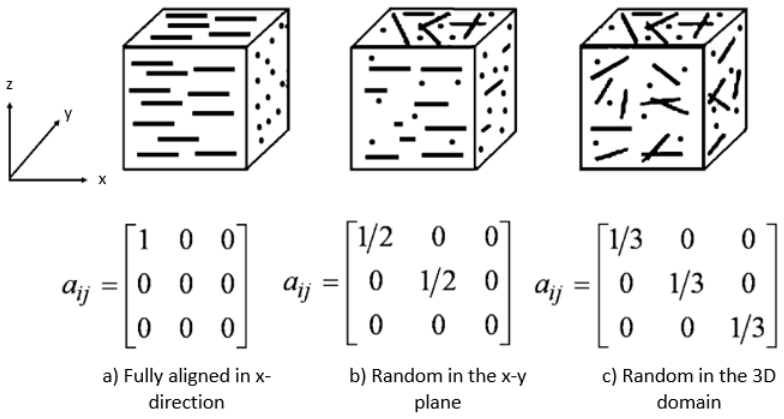

Figure 2.8: Fibre orientation distributions and corresponding second-order tensor components, image from [5].

2.3.2 Homogenization

For fibre-reinforced polymers, the material properties of the composite will be dependent on the fibre and matrix. For such a case, the elastic stiffness tensor C_{ijkl} of the composite forms the relation shown in Equation (2.22) between the average stress and average strain, which are defined in Equation (2.23) and (2.24) respectively [5]. Here, ϕ^f and ϕ^m are the volume fractions for the fibre and matrix while $\overline{\sigma}^f_{ij}$ and $\overline{\sigma}^m_{ij}$ are the stresses for the fibre and matrix, respectively.

$$\bar{\sigma}_{ij} = C_{ijkl}\bar{\epsilon}_{kl} \tag{2.22}$$

$$\bar{\sigma}_{ij} = \phi^f \bar{\sigma}^f_{ij} + \phi^m \bar{\sigma}^m_{ij} \tag{2.23}$$

$$\bar{\epsilon}_{ij} = \phi^f \bar{\epsilon}^f_{ij} + \phi^m \bar{\epsilon}^m_{ij} \tag{2.24}$$

Since the stress and strain of the fibre and matrix can be related respectively, the total average stress for the fibre-reinforced polymer can be obtained according to Equation (2.25).

$$\bar{\sigma}_{ij} = \phi^f C^f_{ijkl}\bar{\epsilon}^f_{kl} + \phi^m C^m_{ijkl}\bar{\epsilon}^m_{kl} \tag{2.25}$$

The average strain of the fibre and matrix can be linked to the average strain of the composite by the strain concentration tensor A_{ijkl}, which is shown for both cases in Equation (2.26) and (2.27), respectively. For the total composite, the elastic stiffness tensor is thus defined according to Equation (2.28), where A_{mnlk} is the only unknown variable.

$$\bar{\epsilon}^f_{ij} = A_{ijkl}\bar{\epsilon}_{kl} \tag{2.26}$$

$$\phi^m \bar{\epsilon}^m_{ij} = (\boldsymbol{I}_{ijkl} - \phi^f A_{ijkl})\bar{\epsilon}_{kl} \tag{2.27}$$

$$C_{ijkl} = C^m_{ijkl} + \phi^f \Big(C^f_{ijmn} - C^m_{ijmn}\Big) A_{mnlk} \tag{2.28}$$

In order to obtain A_{ijkl}, the Mori-Tanaka model, shown in Equation (2.29), was used, where E_{ijkl} is the Eshelby tensor [5].

$$A_{mnkl} = \Big[I_{mnkl} + (1-\phi^f) E_{mnrs}\Big(C^m_{rspq}\Big)^{-1}\Big(C^f_{pqkl} - C^m_{pqkl}\Big)\Big]^{-1} \tag{2.29}$$

3
Discretization

3.1 Process Simulation

The behaviour and properties of polymer materials are sensitive to changes in pressure, volume and temperature. During the injection moulding process the material is subjected to changing conditions regarding all three factors. In order to understand the results obtained from process simulations and to increase the fidelity of the structural model, the underlying mathematical models has to be understood. Thus, the governing equations describing the injection moulding process are presented in this section.

3.1.1 Meshing

The mesh types considered for the process simulation are two-dimensional midplane meshes, see Figure 3.1 a), and three-dimensional solid meshes, see Figure 3.1 b). The midplane mesh type may be suitable for parts for which the thickness is thin throughout the component. It uses the Hele-Shaw approximation, where a thickness is added to replicate the part volume [19]. The solid mesh type on the other hand, is desirable for components with thick features. The three-dimensional solver does not use the Hele-Shaw approximation, but numerically solves the conservation- and constitutive equations.

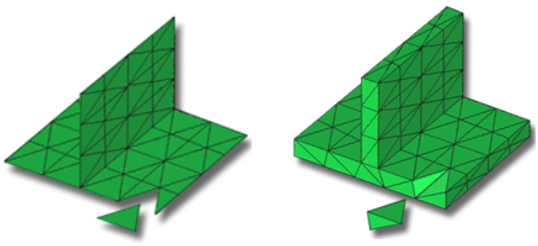

Figure 3.1: Mesh types available for injection moulding simulation, images from [19].

3.1.2 Mathematical Models for Process Simulation

Due to the complexity of the governing equations and injection moulding process, numerical solutions are most often applied. In such cases the governing equations are discretized to form a set of algebraic equations that may solve the non-linear problems of the injection moulding process.

The injection moulding process simulation is most often divided into three parts; the filling and packing stage referred to as the flow analysis, the mould cooling analysis and the structural analysis. However, the mould cooling analysis and the flow analysis are principally coupled since the cavity wall temperature and heat flux are unknown in both cases. [5]

3.1.2.1 Flow Analysis

The filling and packing phases are analysed during the flow analysis, which concerns the flow of liquid plastic into the mould cavity. The flow induced initial stress, i.e. in-cavity residual stress, is also computed during this analysis.

Three-Dimensional Finite Element Method

The governing equations of a moulding system are the conservation laws, i.e. the conservation of mass, momentum and energy that can be derived using the conservation of a control volume. Equation (3.1) presents the conservation of mass, also known as the continuity equation, where ρ is the density, t is the time and $\mathbf{v}$ is the velocity vector. The conservation of momentum is presented in Equation (3.2), for which the gravity g and the shear stress τ is introduced. Considering the conservation of energy, shown in Equation (3.3), T is the temperature field, C_P is the heat capacity, k is the thermal conductivity coefficient, η is the viscosity of the fluid, $\dot{\gamma}$ is the shear rate and ΔH is the heat of generation.

$$\frac{\partial \rho}{\partial t} + \nabla \cdot (\rho \mathbf{v}) = \mathbf{0} \tag{3.1}$$

$$\frac{\partial}{\partial t}(\rho \mathbf{v}) + \nabla \cdot (\rho \mathbf{v}\mathbf{v}) = -\nabla p + \rho \boldsymbol{g} + \nabla \cdot \boldsymbol{\tau} \tag{3.2}$$

$$\frac{\partial}{\partial t}(\rho C_p T) + \nabla \cdot (\rho C_p \mathbf{v} T - k \nabla T) = \eta \dot{\gamma} + \Delta H \tag{3.3}$$

Although these are the governing equations generally considered for injection moulding simulations, it should be noted that for certain processes additional equations may be needed [7].

Since the cavity mould is being filled throughout the flow analysis, the evolution of the melt front has to be advanced. This is done by using the volume of fluid method and solving the transport equation, shown in Equation (3.4), to track the polymer-air interface location [5], [20].

$$\frac{\partial F}{\partial t} + \boldsymbol{u} \cdot \nabla F = 0 \tag{3.4}$$

Using the volume of fluid method, the global domain is divided into control-volumes. Here, F is a concentration function specifying the volume fraction of fluid within a control-volume. Thus, for $F = 0$ the control-volume is considered empty or air filled. However, if $F = 1$ the control volume is fully filled. The melt front is thus located in control-volumes in which $0 < F < 1$ [20].

For each time step Equations (3.1)-(3.3) are computed, after which the melt front is updated according to Equation (3.4). Finally, the material properties are updated accordingly [20].

Two-Dimensional Method

The two-dimensional model uses the Hele-Shaw approximation, where the fluid polymer is assumed to be compressible and filled into a thin cavity. Moreover, since a thin cavity is assumed, inertia effects are disregarded and the polymer is considered to be a viscous fluid [11]. Furthermore, the heat convection in the gap wise direction as well as the heat conduction in the flow direction is neglected. With these assumptions, the continuity equation shown in (3.1) may be rewritten to Equation (3.5) [11].

$$\nabla \cdot (\boldsymbol{v}) = \mathbf{0} \tag{3.5}$$

The above made assumptions also affect the momentum equation. Disregarding the effect of inertia and gravity results in Equation (3.6)-(3.7), where it is reduced to its x- and y-components [11]. Here, u and v are the velocity components in x- and y-direction, respectively.

$$\nabla \cdot \tau = -\nabla p \tag{3.6}$$

$$\begin{aligned} -\frac{\partial p}{\partial x} + \frac{\partial}{\partial z}\left(\eta \frac{\partial u}{\partial z}\right) = 0, \quad x - component \\ -\frac{\partial p}{\partial y} + \frac{\partial}{\partial z}\left(\eta \frac{\partial v}{\partial z}\right) = 0, \quad y - component \end{aligned} \tag{3.7}$$

For the conservation of energy, the rate of gain per internal volume is assumed to be made up of the rate of internal energy input by conduction per unit volume, the reversible rate of internal energy increase per unit volume by compression and the irreversible rate of internal energy increase per unit volume by viscous dissipation [11]. By also disregarding the heat of generations, Equation (3.3) can be rewritten as Equation (3.8) for the midplane approach.

$$\rho C_p = \left(\frac{\partial T}{\partial t} + u\frac{\partial T}{\partial x} + v\frac{\partial T}{\partial y} \right) = k\frac{\partial^2 T}{\partial z^2} + \eta\dot{\gamma}^2 \tag{3.8}$$

3.1.2.2 Mould Cooling Analysis

The governing equation for the temperature field in the mould is the heat conduction equation shown in Equation (3.9), where the thermal diffusivity of the mould α_m is obtained through Equation (3.10) [5], [15]. Moreover, k_M, ρ_M and c_M are the thermal conductivity, density and specific heat of the mould, respectively.

$$\nabla^2 T = \frac{1}{\alpha_M}\frac{\partial T}{\partial t} \tag{3.9}$$

$$\alpha_M = \frac{k_M}{\rho_M c_M} \tag{3.10}$$

3.1.2.3 Structural Analysis for Shrinkage and Warpage

Before an article is removed from the mould, no calculations for the nodal displacements are made. However, thermally and flow induced stresses may be present in the component, causing the initial strain to be non-zero [5]. Assuming the material after ejection is linear elastic, strains are small and that the system remains in internal equilibrium, the relations shown in Equation (3.11) may be used to evaluate the stress-strain components [5], [11], [15]. For this equation, σ_{ij}, σ_{ij}^F, ϵ_{ij}, ϵ_{ij}^{th} and C_{ijkl} are the stress component, initial stress induced by flow, infinitesimal elastic strain component, thermal strain component and elastic material stiffness, respectively. The thermal strain component ϵ_{ij}^{th} due to cooling is obtined from Equation (3.12), where ϵ_{ij}^0, α_{kl} and ΔT are the initial strain from PVT effect, coefficient of linear thermal expansion and temperature difference. For this purpose the elastic strain components are computed in terms of displacement components $\mathbf{u}$, as shown in Equation (3.13) [11].

$$\sigma_{ij} = C_{ijkl}(\epsilon_{kl-\epsilon_{kl}^{th}}) + \sigma_{ij}^F \tag{3.11}$$

$$\epsilon_{kl}^{th} = \epsilon_{kl}^0 + \alpha_{kl}\Delta T \tag{3.12}$$

$$\epsilon_{ij} = \frac{1}{2}(u_{i,j} + u_{j,i}) \tag{3.13}$$

For a midplane analysis the computation of thermally and flow induced stresses may be simplified by assuming that in the case of the x_3-direction being normal to the local midplane, the shear strains $\epsilon_{13} = \epsilon_{23} = 0$. Furthermore, the normal stress σ_{33} is constant across the assigned thickness h. This is valid under the assumption that $\sigma_{33} < 0$. Moreover the part may be considered fully constrained within the plane before ejected. Thus, only ϵ_{33} would be non-zero before ejection. [5]

3.2 Sun Simulation

Exposure to sun loads may cause heat build up in the vehicle cabin, which can significantly affect the lifetime and appearance of interior components [4]. Furthermore, the thermal load can cause deformations in the material. The deformations from heat exposure may cause thermal expansion according to Equation (3.12). In addition, the strain can give rise to stresses within the material, as shown in Equation (3.11).

The thermal loads used for this thesis have been generated in a different thesis work carried out for the same project. For this purpose, the software TAITherm was used to compute the thermal load, applied at each node of the full car model, from weather data [4]. The software is specifically designed to compute thermal loads on complex geometries and takes conduction, convection and radiation into consideration, which all affect the response from interior trim components.

Furthermore, it should be noted that the thermal loads obtained represent 6 months of active usage of the vehicle. Thus, the car is considered to be moved and rotated during the simulation, which causes a transient thermal load that allows for intermediate cooling [4]. The weather data used as input in the modeling is collected by the American Weather institute in Phoenix. The data measured by Volvo in the physical experiment is also collected in Phoenix, U.S.A. However, the geographical locations for measurements are not the exact same [4]. It should also be noted that the heading of the vehicle used for collecting measurements is not the same as for the one being simulated. Nevertheless, previous work found that the results obtained gave a reasonable prediction of the thermal loads, although somewhat lower than for the physical test [4]. This can be explained by the fact that the physical test was carried out for a stationary vehicle whereas the simulated response was carried out with consideration to customer usage.

4
Simulation Workflow

In order to solve the flow-, structural- and cooling analyses associated with the process simulation for injection moulding, different software have been tried in order to find an appropriate workflow that provides desired results. The results obtained can be used to improve the fidelity of the sun simulation performed on the full car model. For this thesis the software examined for process simulation were Moldflow, Moldex3D and DigimatRP.

The mesh used for structural analysis is made up of quadratic shell elements. While DigimatRP allows for such elements to be used, Moldflow and Moldex3D allow usage of only one-dimensional elements, triangular elements or tetrahedral solid elements. As a result, different mapping solutions were investigated. The software considered for obtaining a mapping function were DigimatMAP and DigimatRP as well as the BETA/Ansa Result Mapper function. Furthermore, the Abaqus solver was used for the structural analysis together with the BETA Ansa/Meta pre- and post-processors.

4.1 Workflow

An overview of possible workflows is presented in Figure 4.1. Areas marked in grey represent the stages in the manufacturing process that are simulated, while the areas marked in green denote how the component is affected by the manufacturing phase. Furthermore, areas marked in yellow and red show the obtainable data from the different steps in the manufacturing process. Each process simulation output box is marked with the name of the software that may provide the data within the box.

The goal is to capture all steps in the life of the component, from manufacturing to sun exposure. Thus, the steps not simulated in a process simulation tool has to be accounted for in the structural solver. For example, if the in-cavity stress is used as an output from the process simulation, then the ejection- and relaxation process has to be simulated in the structural solver before application of the sun load. Moreover, if only the injection process is simulated in the process simulation tool, the cooling process must be added to the steps carried out in the structural solver.

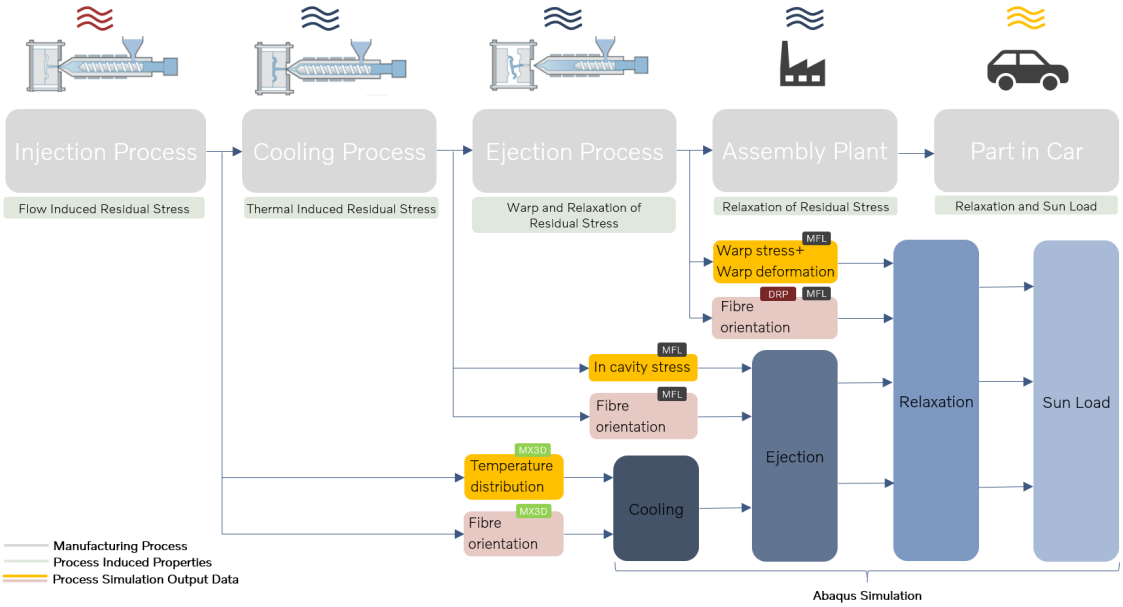

Figure 4.1: The simulation process for one component with obtainable data from process simulation tools.

Moldex3D offers to output the temperature distribution throughout the component after the injection process, from which stresses can be calculated. Using such data requires the cooling and ejection process to be simulated in Abaqus. The ejection process can be replicated in the structural solver by the release of fully constrained nodes, which allows stresses to alter and deformations to form [8]. However, simulating the cooling in the structural solver is challenging, since the placement of cooling channels highly affects the results, something which is difficult to model in the structural solver [5], [7]. Moldflow and DigimatRP allows to export data after the ejection process has been simulated. The use of such data requires not only stresses, but also data that describes the deformation of the component to be exported, since the relaxation causes warpage. This gives rise to several difficulties, determining the state of relaxation being one. Moreover, a deformed mesh may cause components to overlap in an unlikely way when imported into the full car model. It was thus desired to use the stress data obtained after the in-mould cooling had been simulated in the process simulation tool. As a result, the ejection and relaxation process had to be simulated in Abaqus before carrying out the sun simulation.

Apart from evaluating the desired data output, the approach of using a midplane approximation and solid element mesh have been investigated. From a computational point of view, the three-dimensional element mesh type is expected to give more accurate results, since the in-thickness flow direction is disregarded in the midplane approximation. Moreover, some components have complex geometries, which can be challenging for the approximation [5]. On the other hand, many trim components can be considered thin walled, which is a presumption for the midplane approximation. From a practical point of view a midplane approximation may be favorable, since the mesh used for structural analysis can be used also in the process simulation tool. Instead of creating 3D representations of components, which are needed for the

solid element mesh to be created in the process simulation tool, the only operation needed is to divide all quadratic elements into two triangular elements. This can easily be done in the Ansa pre-processing tool and can save computational time. Unfortunately, no suitable mapping integration for either Moldflow or Moldex3D was found for the midplane approximation. DigimatRP however, did allow for the quadratic shell element mesh to be used for process simulation. Furthermore, the built in mapping function allow data to be mapped directly in the process simulation software. Unfortunately, the software only has the function of predicting fibre orientations and cannot output the residual stresses.

4.2 Final Methodology

For the final workflow, the stresses and fibre orientations were exported after performing the injection- and cooling simulation in the process simulation tool. Here, the Moldflow software was used to obtain the process induced data. For the test component, the material *Schulamid 6 GF 30H* was used with process parameters set according to Moldflow propositions. Thus, the mould surface temperature was set to 60°C and the melt temperature to 260°C. The filling pressure was ramped to 80 MPa during 10 seconds. For the full car analysis, the materials were chosen as presented in Figure 1.1 and process parameters were set according to Moldflow-suggested material specifications.

Since the in-cavity stress was used, the ejection and relaxation was simulated in the structural solver before performing the sun analysis. For the simulation of the ejection and relaxation, the component is considered to be fully constrained in the mould. Furthermore, it is assumed that there is no in-mould shrinkage. The in-cavity stresses can be seen as recorded frozen pressure at each node after the cooling has been performed [8]. During the simulation, the mould boundary constraints are released and set to the constraints used for in-car mounting. This allows the component to deform and the stresses to alter accordingly.

As the recorded in-cavity stresses were above or close to the yield stress for many of the components, an elastic material model was used. This enabled the stresses to find an equilibrium after releasing the in-mould boundary conditions. Since the sun loads are not big enough to cause large deformations, or plasticity at all, this simplification was considered acceptable.

In order to find the appropriate time allowed for relaxation a test was made for 100 hours of relaxation. Figure 4.2 shows the von Mises stress for a control node placed in the centre of the test component. It can be seen that the largest decrease in stress occur instantaneously after the constraints have been released. As the model is purely elastic with creep, the stress continues to decrease as time passes. However, the rate in which the stress decreases significantly drops with time.

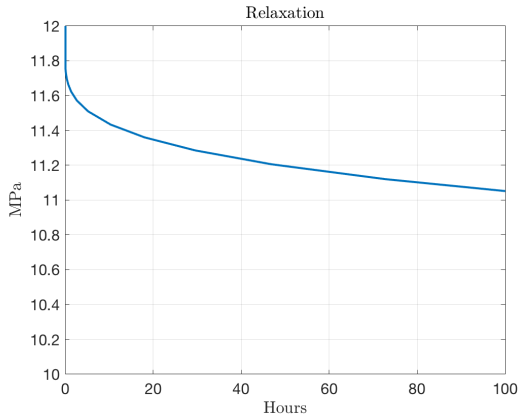

Figure 4.2: Von Mises stress during 100 hours of relaxation.

The rate of stress decrease is presented in Figure 4.3. It can be seen that after 50 hours the rate is close to constant, with a value of approximately -0.004. Thus, 50 hours of relaxation was allowed before applying the sun load. The simulation of the ejection and relaxation phases were carried out as separate steps in the complete car model before the thermal load was applied.

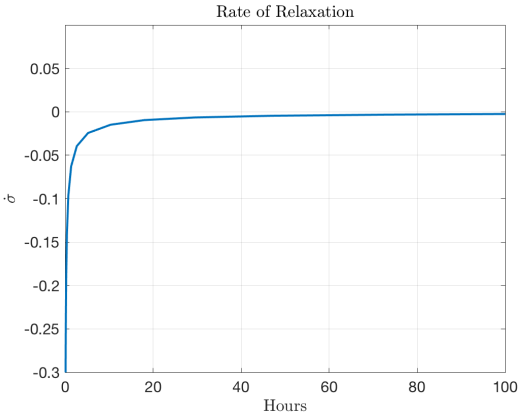

Figure 4.3: Rate of decreasing von Mises stress during 100 hours of relaxation.

The sun load was represented by thermal loads computed in TAITherm, which were obtained through weather data with consideration to active usage of the vehicle. First, the temperature of all components was ramped up to 23°C. After this, the transient thermal loads were applied, before ramping the temperature down. Finally, the results were imported into the Meta post-processing tool, where results were analyszed.

The developed workflow can be seen in Figure 4.4. First, each component for which the process induced parameters are to be computed, is volumized. For the test component a thickness of 3 mm was used. The volumized part is then used to create a surface representation, which can be exported to Moldflow as a *.step file.

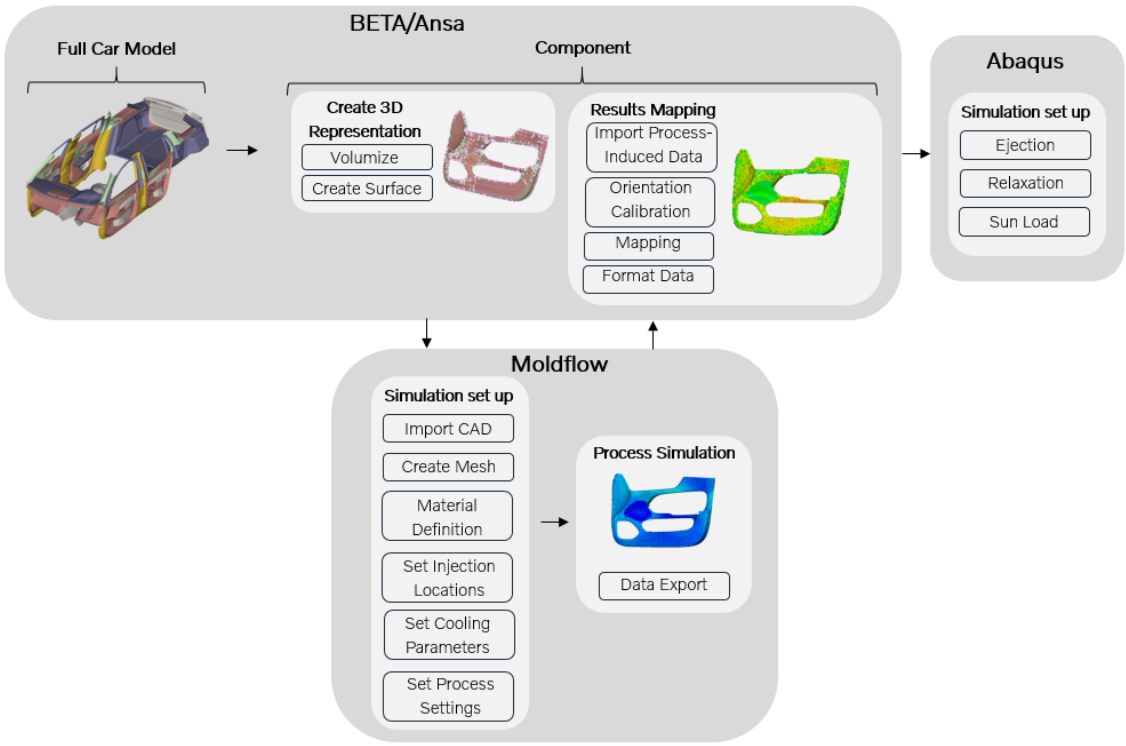

Figure 4.4: The developed workflow for the chain of simulations. The upper left box represents operations carried out component-wise in the full car model and the lower box represents component-wise process simulation. The upper right box represents the structural analysis carried out on the complete car model.

After importing the surface representation a mesh is created. Thereafter, the injection locations as well as process settings are set, after which the injection moulding simulation can be carried out. The process induced stresses and fibre orientations are exported as *.xml files together with the model, which is exported as a *.udm file. The results are mapped to the mesh used for structural analysis by the use of the Ansa pre-processing results mapping tool. Finally, the structural analysis can be performed as explained earlier in this section.

5
Analysis

In order to assess the performance of the chosen workflow, as well as to investigate possible improvements for future development, the effect of implementing alternative approaches has to be evaluated. Thus, the effect of implementing the midplane approximation and three-dimensional solution for the process simulation is studied. Furthermore, the performance of the mapping tool is evaluated by assessing the effect the tool has on the data. Moreover, the simulation of the relaxation phase has to be understood. The results obtained after performing the ejection and relaxation simulation in Abaqus are thus compared to the same when computed in Moldflow. Finally, the effect of the process induced parameters on the complete car sun simulation is analysed.

5.1 Process Study

For the evaluation of midplane- and solid element approach, an analysis was made in Moldflow for both cases. Here, the test component was used for simulation with the material *Schulamid 6 GF 30H* and process parameters as described in Section 4.2. Figure 5.1 shows the von Mises residual stress after warpage for both cases. It can be seen that a similar stress distribution is predicted for both methods. However, the area close to the gate position on the right boundary of the component, marked with a yellow cone, shows lower stress values for the midplane approximation. Here, a difference of approximately 10 MPa can be seen. Considering the areas above and below the injection location, somewhat lower stresses can be seen for the analysis carried out with the solid element mesh type.

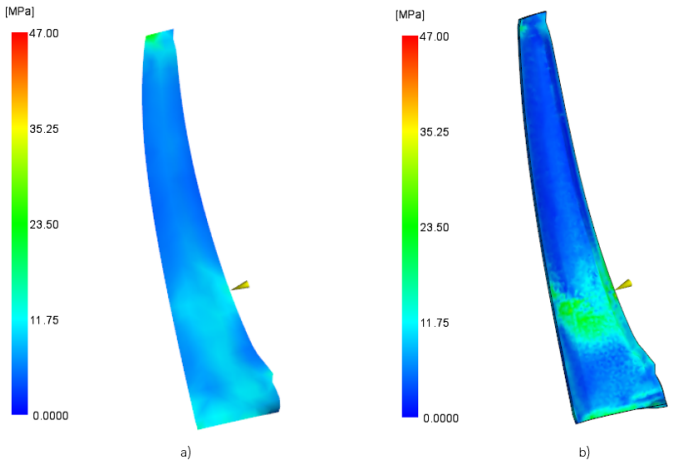

Figure 5.1: The von Mises stress distribution for the test component obtained via process simulation using a) a midplane mesh and b) solid element mesh.

Figure 5.2 presents the displacement magnitude for both cases. As for the stress distribution, similar trends can be seen for the displacement magnitude. Differences occur close to the gate location as well as near the lower left edge of the component.

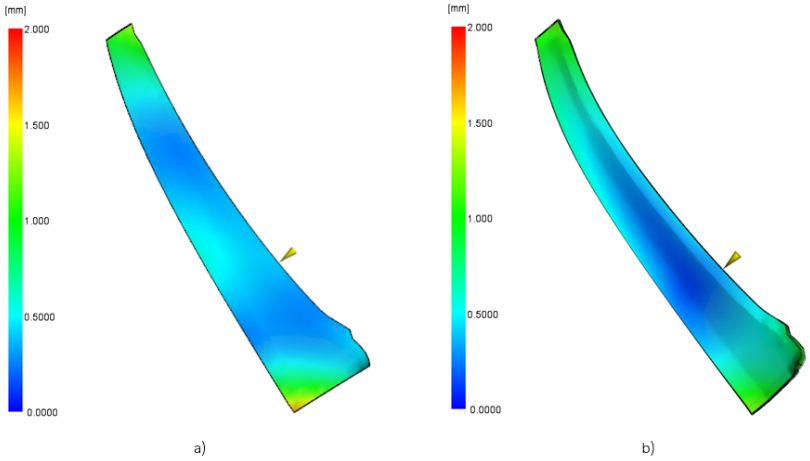

Figure 5.2: The deflection magnitude for the test component obtained via process simulation using a) a midplane mesh and b) solid element mesh.

The chosen approach also has an effect on fibre orientations. Figure 5.3 presents the fibre orientation tensor for both cases. It should be noted that the figure presenting fibre orientations for the three-dimensional approach, shows results for all layers through the thickness, while the midplane approach shows values only for the midplane. It can be seen that the fibre orientations show similar patterns. However, higher values are observed for the midplane approach in the upper region of the component.

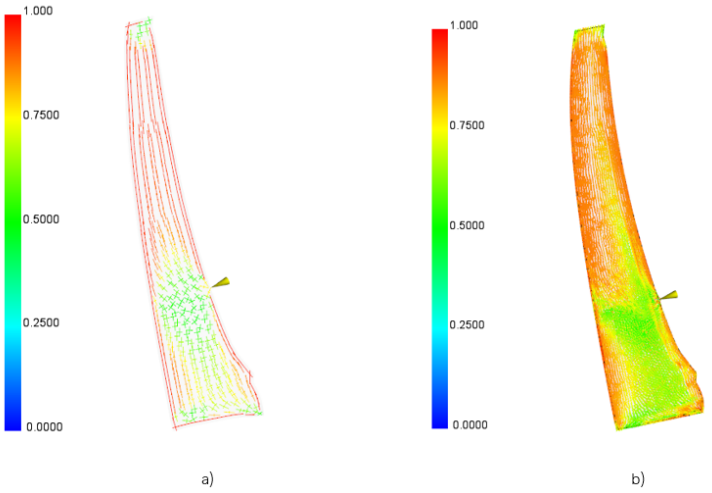

Figure 5.3: The the fibre orientation tensor for the test component obtained via process simulation using a) a midplane mesh and b) solid element mesh.

For evaluating the mapping tool, the results obtained from Moldflow were mapped to the structural mesh. This was done for the in-cavity stresses as well as for the fibre orientations. The data was obtained from the analysis carried out for the test component, when using the solid element mesh approach. Figure 5.4 shows the residual von Mises stress tensor for both cases. Values of the same magnitude can be seen in both figures. However, while the Moldflow model shows stress values of around 10-12 MPa, the results on the mapped mesh are roughly twice as big.

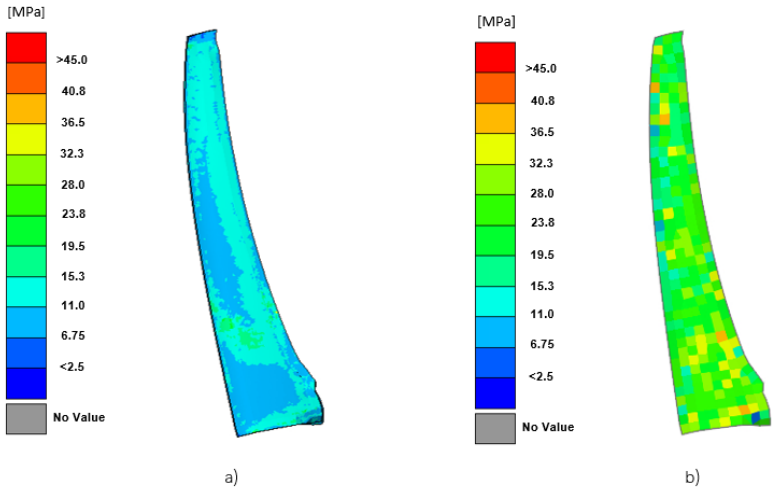

Figure 5.4: The von Mises representation of the stress tensor for the test component from a) Moldflow and b) after mapping in Ansa, i.e. the average through the thickness.

In order to visualize the difference between the models, a probe test was made for the outer right boundary of the test component, as seen in Appendix B.1. The results are shown in Figure 5.5, where the stress values along the boundary are presented for both cases. The stresses are generally somewhat higher for the Abaqus model along the boundary. However, the size of the difference varies.

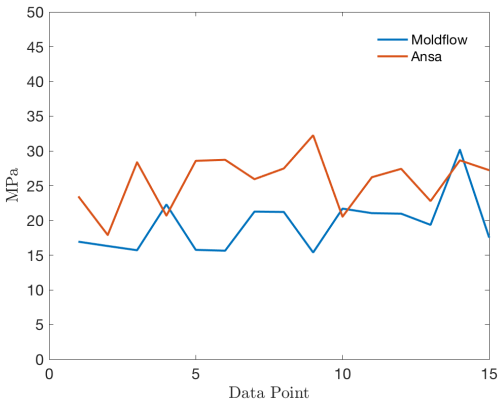

Figure 5.5: Residual von Mises stress values along right outer boundary of the test component for Moldflow results and mapped correspondence in Ansa.

For comparison of the fibre orientations, the average fibre orientation from Moldflow was used, since the current mapping tool uses the average value through the thickness. Figure 5.6 a) shows the average fibre orientations while Figure 5.6 b) presents the corresponding mapped data. The mapped data matches the average fibre orientation well. Moreover, when comparing both the average fibre orientation and the mapped data to the fibre orientation tensor obtained from Moldflow, presented in Figure 5.3 b), a good correlation can be seen. It should be noted that the data from Moldflow is obtained by use of the probability density function as explained in section 2.3.1. The mapping function considers the values to be valid, why there is no probability bar for the mapped data.

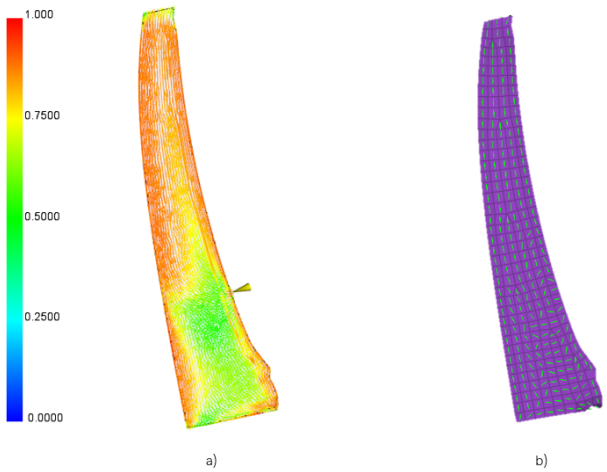

Figure 5.6: The average fibre orientation for the test component from a) Moldflow and b) after mapping in Ansa.

In the chosen workflow the simulation of the relaxation phase is carried out in Abaqus. As mentioned, the alternative approach is to simulate the same in Moldflow. It is thus important to asses the response after relaxation for both cases in order to understand the differences. Figure 5.7 presents the residual von Mises stress distribution for both approaches. It can be seen that the stresses in the upper and lower region of the component are higher when simulating the relaxation in Abaqus.

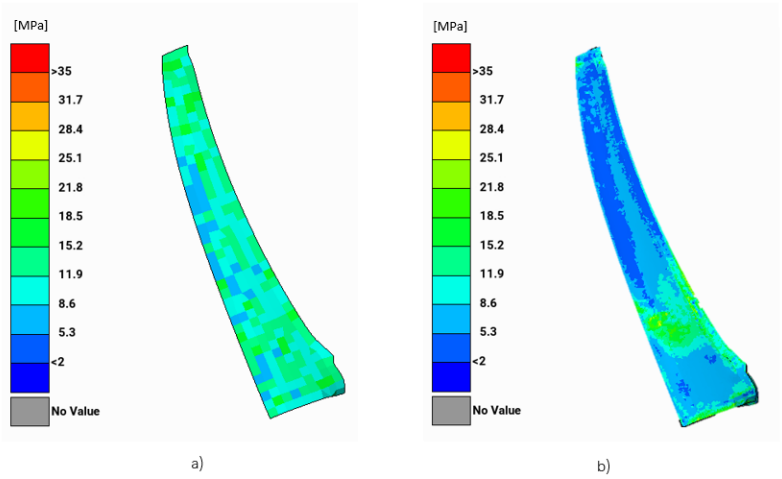

Figure 5.7: Residual von Mises stress distribution after warpage for relaxation carried out in a) Abaqus and b) Moldflow.

In order to visualize the differences between the two approaches, a measurement was taken along the right outer boundary of the test component, seen in Appendix B.1. The results are shown in Figure 5.8, where it can be seen that the stresses obtained after simulating the relaxation in Abaqus are approximately 10 MPa higher than the results obtained from Moldflow.

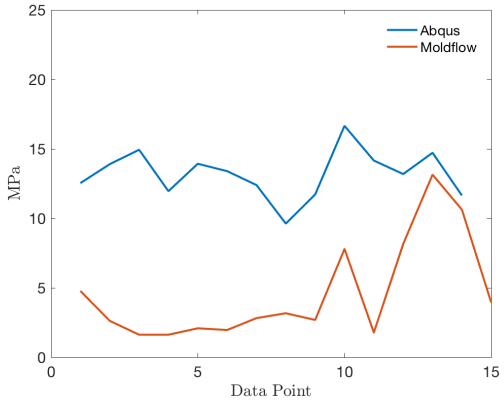

Figure 5.8: Residual von Mises stress values along right outer boundary of the test component, starting from the top, with relaxation carried out in Abaqus and Moldflow.

The displacement field after relaxation is presented for both cases in Figure 5.9, where values of similar magnitude can be seen. However, the distribution is different between the models. In the Abaqus model the deflection increases in the upper region and shows a minimum value at the lower left edge. The Moldflow model shows a minimum value in the centre of the component. For latter case the displacements increase in all directions when moving away from the centre.

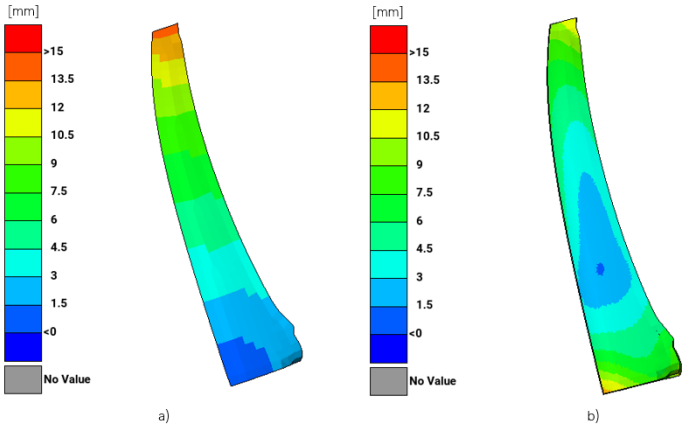

Figure 5.9: Deflection magnitude after warpage for relaxation carried out in a) Abaqus and b) Moldflow.

5.2 Modelling Study

In order to examine the effect of the process induced parameters on the structural analysis, a sun simulation was made on a complete car model for 6 months of transient thermal load. One simulation was carried out with consideration to process induced stresses and fibre orientations and one without the process induced parameters included. Figure 5.10 presents the residual stresses obtained after the sun simulation for both cases. It can be seen that the resulting stresses are generally higher when taking the process induced parameters into account.

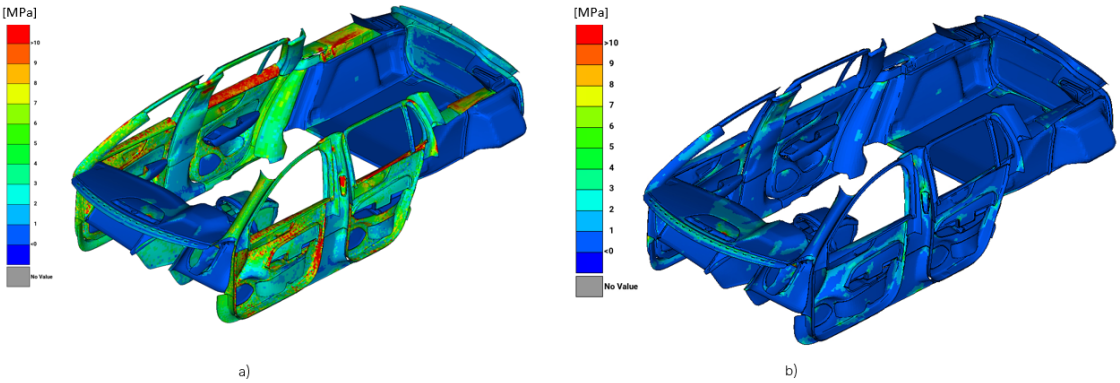

Figure 5.10: Residual von Mises stresses obtained from sun simulation carried on out on a) full car model with process induced parameters and b) full car model without process induced parameters.

The displacement field obtained after carrying out the sun simulation can be seen in Figure 5.11 for the same two cases. The results from the analysis made with consideration to the process induced parameters again show higher values. Furthermore, components expected to have large exposure to the sun light seem to deflect more than components with low thermal exposure.

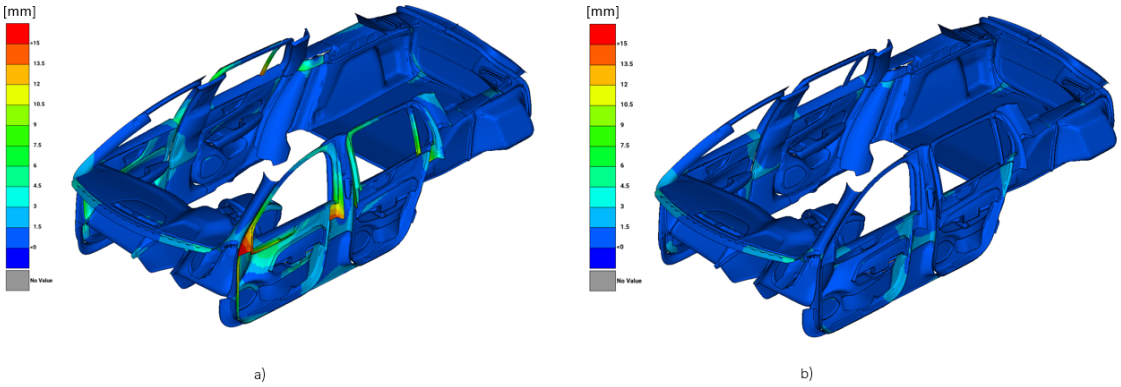

Figure 5.11: Total nodal displacement obtained from sun simulation carried on out on a) full car model with process induced parameters and b) full car model without process induced parameters.

Critical locations to be considered are areas close to the windows of the vehicle, as they are directly exposed to the sun light. Thus, the results for the upper A-pillar, front window concealing panel, upper door panel and tailgate panel are further evaluated. This is done by visualizing the total displacement and von Mises stress along the boundary lines specified in Figure 5.12. The measurement locations are presented thoroughly for each component in Appendix B.2-B.5.

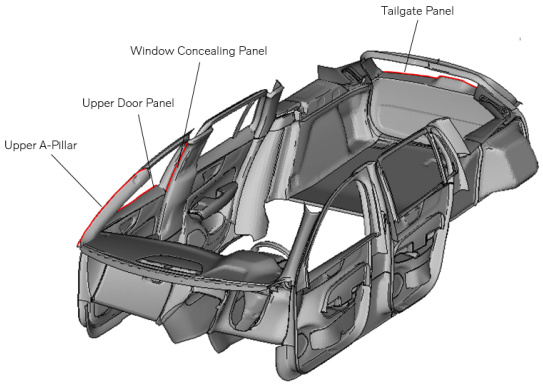

Figure 5.12: Boundary lines used for comparison of results obtained from sun simulation with- and without consideration to process induced parameters.

Figure 5.13 shows the results along the boundary line of the front upper A-pillar. The displacements are similar, although the case without process induced parameters deflects approximately 0.6 mm more at the end of the measurement line. On the other hand, the von Mises stresses are higher throughout the measurement for the case with process induced parameters taken into account.

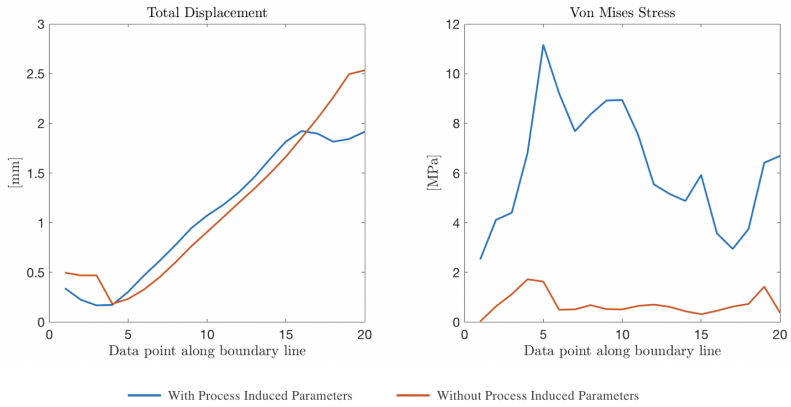

Figure 5.13: Total displacement and von Mises stress distribution after sun simulation along the boundary line for the front upper A-pillar.

The total nodal displacement for the front window concealing panel, as seen in Figure 5.14, is highly affected by the process induced stresses and fibre orientations. The total displacement does not only reach higher values, but is also distributed differently over the considered boundary line. The most extreme point shows a total displacement of 8 mm for the simulation with process induced parameters. Without the induced parameters taken into account the same measurement is approximately 0.5 mm. The von Mises stress along the boundary line is also generally higher for the former case, with a peak value of 3 MPa. The latter case reaches only 0.1 MPa.

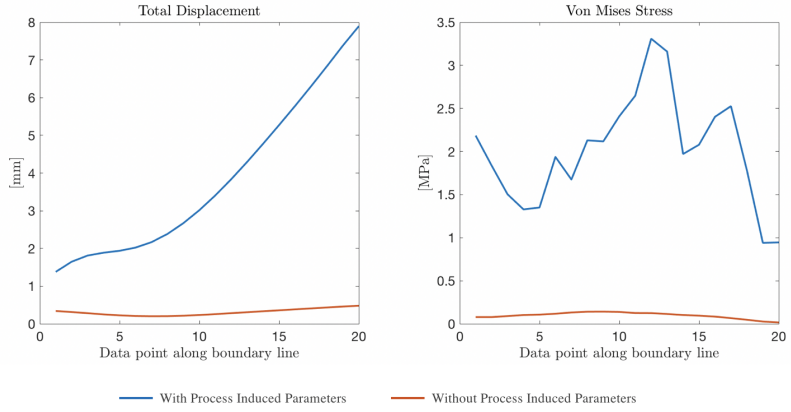

Figure 5.14: Total displacement and von Mises stress distribution after sun simulation along the boundary line for the front window concealing panel.

As for the front window concealing panel, the results obtained for the front upper door panel, presented in Figure 5.15, show higher values when process induced parameters are used as initial conditions. The von Mises stress distribution shows a peak value of 9 MPa for the results obtained with process induced parameters. For the case without induced parameters the stress distribution is close to zero across the entire measurement line. The displacement show similar trends for both cases. However, the displacements are somewhat higher for the simulation with process induced parameters.

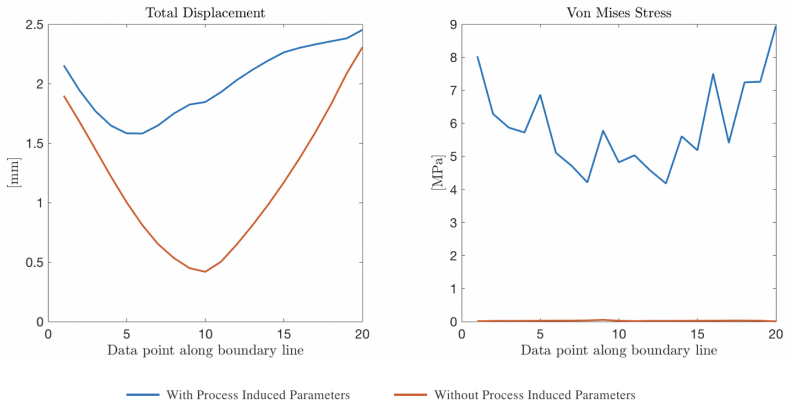

Figure 5.15: Total displacement and von Mises stress distribution after sun simulation along the boundary line for the front upper door panel.

The results obtained from the measurement on the tailgate panel are shown in Figure 5.16. The displacements coincide close to the edges of the panel. However, they deviate by approximately 1 mm in the centre of tailgate panel. The stresses are up to 3 MPa higher when process induced parameters are taken into account.

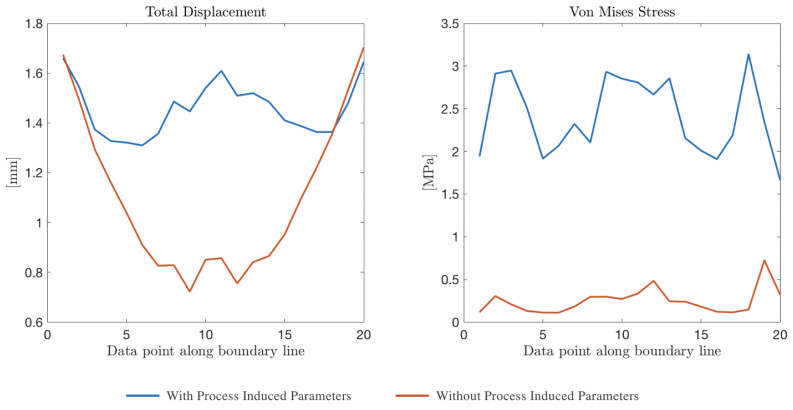

Figure 5.16: Total displacement and von Mises stress distribution after sun simulation along the boundary line for the tailgate panel.

6

Discussion and Concluding Remarks

In order to provide an overview of the developed workflow and of its benefits as well as disadvantages, the analysis of results are first discussed, after which the workflow itself is considered. Finally, recommendations for future work are presented.

6.1 Simulation Results

Similar trends can be seen for the three-dimensional model and midplane approximation when comparing the stress distribution and displacement magnitude over the test component after process simulation. Differences occur in areas close to the inlet and where the component bends. A reason for such results may be explained by the assumptions made for the Hele-Shaw midplane approximation. It is a assumed that the cross sectional area of the component is thin and that flow is allowed only in two directions. As seen by the results, good correlation can be obtained in areas that fulfill the requirements. However, in areas where the assumptions are not fully attained, such as in turbulent flow regions, where components bend and where the thickness increases, the results seem to deviate. Furthermore, it should be noted that the same trends can be seen for the fibre orientation tensor. While some interior trim components have complex geometries, many fulfill the assumption of having a thin cross sectional area. If possible, the midplane approximation should be considered for practical use, since it may save computational time.

An important part of increasing the fidelity of the sun simulation is to have correct data. The process study showed that the developed mapping tool, which was used to transfer the process induced parameters to the mesh used for structural analysis, had an effect on the data. A considerably good correlation was seen for the fibre orientations while the in-cavity stresses showed deviations of up to approximately 10-15 MPa. Currently, the tool uses the average value through the thickness of the component, and interpolates over the mesh. The mapped data is thus mesh dependent, which may cause the stresses designated to some elements to deviate.

The effect of simulating the relaxation in Abaqus as opposed to Moldflow showed similar trends for the residual stresses while the displacement distribution did not correlate. Moreover, the Abaqus model generally showed higher stress and displacement values. One reason for this may be the difference in element size, where a

coarse mesh gives a stiffer response. Furthermore, it should be noted that the results depend on the boundary conditions. The Abaqus model was constrained according to its mounting solution in the vehicle whereas the component was considered to be isolated in the Moldflow model. This affects the allowed displacement direction and magnitude. Another important factor to consider is the length of the relaxation step. The relaxation in Abaqus was carried out for 50 hours, after which the rate of the decrease in stresses had dropped considerably. The time considered for relaxation in Moldflow is unknown and may have an effect on the results obtained. Furthermore, the material model used in the simulation made in Abaqus is based on empirical data, whereas the Moldflow material model is not, which also may affect the results obtained.

6.2 Workflow

The proposed methodology, presented in Figure 4.4, does meet the objectives as the sun simulation can be made with process induced parameters taken into account. Nevertheless, some simplifications were made to enable the workflow to be completed in the scope of this thesis. The two major factors identified, affecting both the workflow and the results obtained from the chain of simulations, is the choice of mesh type for the process simulation and the mapping function. The choice of implementing either the midplane Hele-Shaw approximation or the three-dimensional solution has been discussed in earlier sections. While the former may be suitable for many components, difficulties may occur for complex geometries. From a practical point of view, such an approximation would be valuable as it would save computational time. Additionally, the mesh used for the structural analysis can be used also for the process simulation when implementing the midplane approximation, thus saving extra computational time. Unfortunately, no software provided functions for data from the midplane analysis to be transferred to the structural solver. Thus, the solid mesh type approach was implemented.

The mapping function works well from a practical point of view, since data for specific components can be mapped directly to the complete car model. The mapped data corresponds reasonably well to both the fibre orientation and in-cavity stresses from Moldflow. However, an implementation of a complete homogenisation tool for the fibre orientation data, as opposed to using the average orientation through the thickness, can improve the fidelity of the structural analysis.

6.3 Future Work

Results have shown that the data obtained from the midplane approach correlates reasonably well to the parameters from the three-dimensional process simulation. A reason for this is that the component compared is thin-walled and relatively flat. Most trim components used in the full car model can be considered to be thin-walled. Nevertheless, some do have more complex geometries, which may invalidate results obtained from the midplane approach. In order to assess the effect of the midplane

simplification on the final results, a comparison between both models can be done for the sun simulation of the complete car model.

To use the midplane simplification would streamline the workflow. With a midplane approximation the mesh used for structural analysis can also be used in the process simulation. It should be noted, that mapping of process induced data to the structural mesh is still beneficial compared to import of the part with the process induced data back into the full car model. In such a case boundary conditions need to be formed for the newly imported component. Thus, the process of mapping is more time efficient, and allows for fewer mistakes to be made, since the transition of data is less. Furthermore, the use of a midplane approximation can save computational time, both since no new mesh needs to be generated and since the process simulation itself requires less time.

Another factor to take into consideration for increasing the fidelity of process simulation and thus the complete car sun simulation, are the process parameters. Previous work has shown that these parameters have a significant impact on the results, why they need to be taken into consideration [9]. Thus, to increase the fidelity of the the model, the accuracy of the chosen parameters should be increased. Parameters affecting the flow rate, packing pressure, melt- and cooling of the component are of great importance.

The results obtained from the simulation of the relaxation stage in Abaqus showed a stress distribution similar to the result obtained for the Moldflow model. However, the stress values were higher for the results obtained from Abaqus. The displacement distribution did not correlate. As explained, the boundary conditions may have an effect on the results. Another reason may be the differences in the material models. Further evaluation may thus be necessary in order to validate the results.

Finally, the effect of the assumptions made needs to be investigated in order to increase the fidelity of the model. For example, the current mapping tool uses average material orientations. The accuracy is expected to increase with a complete homogenization tool. Furthermore, the nodal displacements are set to zero during the time for which the component is considered to be in the mould. However, a small displacement can have a large impact on the in-cavity stresses. In reality, both the mould and component will deflect somewhat even before ejection. By using a contact definition the displacement can be captured.

To conclude, a workflow has successfully been developed that allows process induced parameters to be taken into account for sun simulation of a complete car model. By integrating the process simulation and mapping results to the structural mesh, the fidelity of the sun simulation can be improved. Furthermore, the same workflow can be used also for other types of structural analyses.

Bibliography

[1] B. D. Agarwal, L. J. Broutman, and K. Chandrashekhara,
Analysis and Performance of Fiber Composites, 4th ed.
John Wiley & Sons, 2006.

[2] A. Patil, A. Patel, and R. Purohit, "An overview of polymeric materials for automotive applications,"
Materials Today: Proceedings, vol. 4, pp. 3807–3815, 2017.

[3] N. McCrum, C. Buckley, and C. Bucknall.,
Principles of polymer engineering, 2nd ed. Oxford Univ. Press, 1997.

[4] K. Staffas, "Cae sun simulation - thermo structural coupling,"
Royal Institute of Technology, School of Enginnering Sciences, 2020.

[5] R. Zhen, R. I. Tanner, and X.-J. Fan,
Injection Molding - Integration of Theory and Molding Methods.
Springer, 2011.

[6] K. Beomkeun and M. Juwon, "Residual stress distributions and their influence on post-manufacturing deformation of injection-molded plastic parts,"
Journal of Materials Processing Technology, vol. 245, pp. 215–226, 2017.

[7] M.-L. Wang, R.-Y. Chang, and C.-H. Hsu,
Molding Simulation - Theory and Practice. Hanser Publishers, 2015.

[8] Z. Fan, H. Yu, Z. Zuo, and R. Speight, "Anisotropic thermo-viscous-elastic residual stress model for warp simulation of injection molded parts,"
SPE ANTEC Anaheim, 2017.

[9] A. Östergren, "Prediction of residual stresses in injection moulded parts,"
Chalmers University of Technology, 2013.

[10] J. Kihlander, "Finite element simulation of vibrating plastic components,"
Chalmers University of Technology, 2013.

[11] Moldex3D, *User Manual*, link:
http://support.moldex3d.com/2020/en/usermanual.html[2021-05-01]., 2020.

[12] W. D. Callister and D. G. Rethwisch,
Materials Science and Engineering an Introduction, eighth.
John Wiley & Sons, 2009.

[13] K. Carr, "Difference between linear & branched polymers," *Sciencing*, 2018. [Online]. Available: `https://sciencing.com/difference-between-linear-branched-polymers-8521652.html`.

[14] P. H. Kauffer, *Injection Molding : Process, Design, and Applications*. Nova Science Publishers, Incorporated, 2010.

[15] Autodesk, *Autodesk User's Guide*, link: https://help.autodesk.com/view/MFIA/2021/ENU/[2021-04-29]., 2021.

[16] T. Sato and S. Richardson, "Numerical simulation of the fountain flow problem for viscoelastic fluids," *Polymer Engineering and Science*, vol. 35, pp. 805–812, 1995.

[17] F. P. Baaijens and L. P. Douven, "Calculation of flow-induced residual stresses in injection moulded products," *Applied Scientific Research*, vol. 48, pp. 141–157, 1994.

[18] Omnexus, *Coefficient of Linear Thermal Expansion*, link: https://omnexus.specialchem.com/polymer-properties/properties/coefficient-of-linear-thermal-expansion [2021-05-10]., 2021.

[19] Autodesk, *Features Simulation tools for plastic injection molding*, link: https://https://www.autodesk.com/products/moldflow/features/ [2021-05-05]., 2021.

[20] S.-W. Kim and L.-S. Turng, "Developments of three-dimensional computer-aided engineering simulation for injection moulding," *Modelling and Simulation in Materials Science and Engineering*, vol. 12, pp. 151–173, 2004.

A

PVT Diagrams for Materials Used in Full Car Sun Simulation

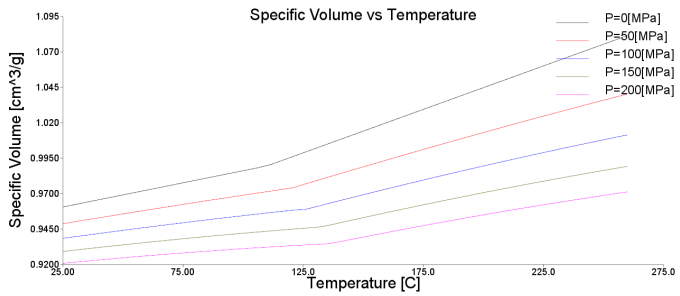

Figure A.1: PVT diagram for ABS(Ver1).

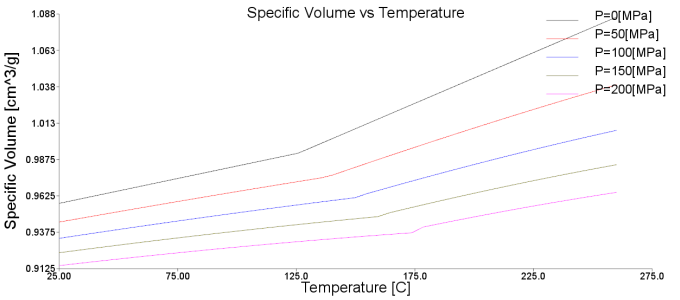

Figure A.2: PVT diagram for ABS(Ver2).

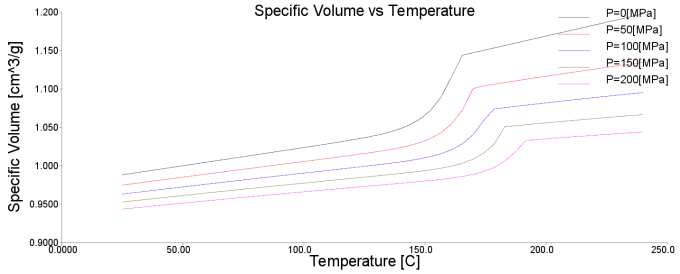

Figure A.3: PVT diagram for PP-T15.

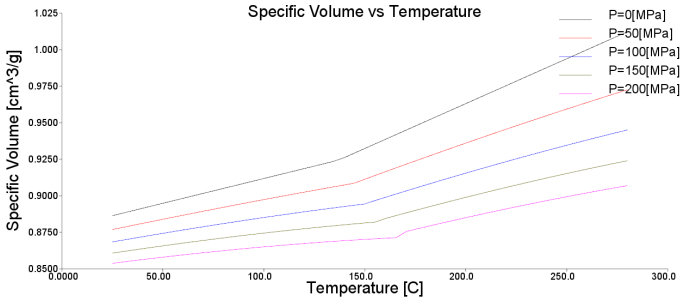

Figure A.4: PVT diagram for PC+ABS(85%PC).

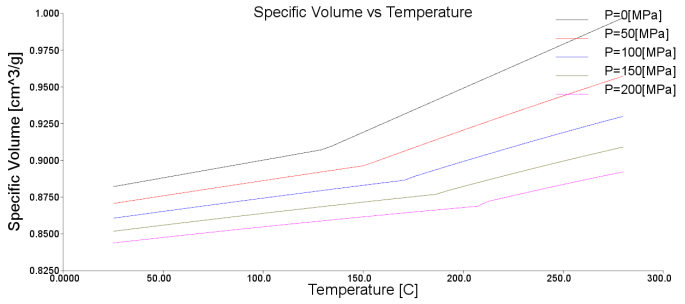

Figure A.5: PVT diagram for PC+ABS(65%PC).

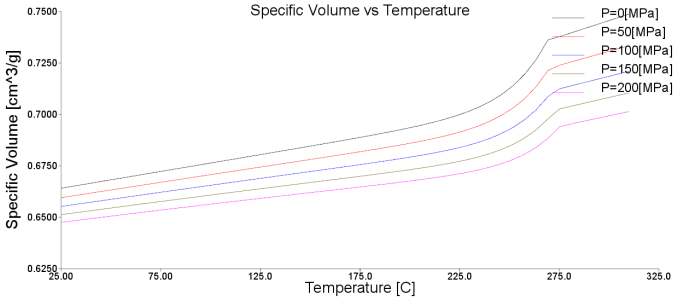

Figure A.6: PVT diagram for PPGF30.

B

Boundary Lines Used for Measurment on Specific Components

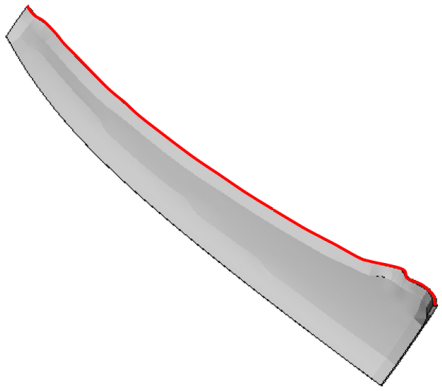

Figure B.1: Boundary line on lower a-pillar used for comparison of the developed mapping tool.

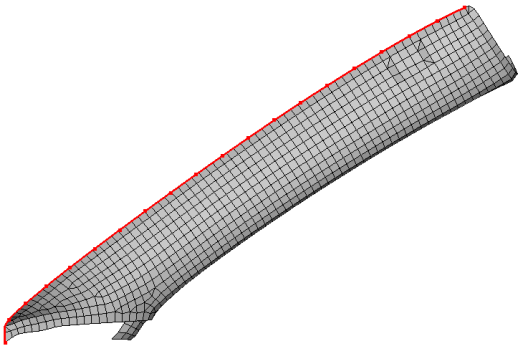

Figure B.2: Boundary line on upper a-pillar used for analysis of results obtained from sun simulation.

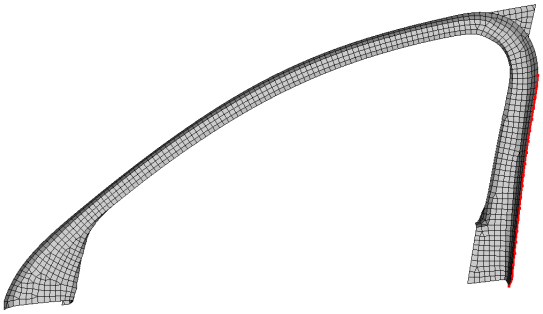

Figure B.3: Boundary line on front window concealing panel used for analysis of results obtained from sun simulation.

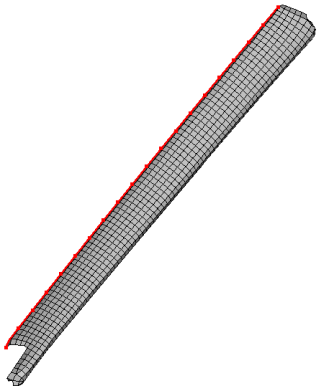

Figure B.4: Boundary line on upper door panel used for analysis of results obtained from sun simulation.

Figure B.5: Boundary line on tailgate panel used for analysis of results obtained from sun simulation.

DEPARTMENT OF INDUSTRIAL AND MATERIALS SCIENCE
CHALMERS UNIVERSITY OF TECHNOLOGY
Gothenburg, Sweden
www.chalmers.se

CHALMERS
UNIVERSITY OF TECHNOLOGY